

STRUCTURAL AND OPTOELECTRONIC PROPERTIES OF SOL-GEL  
DERIVED NICKEL OXIDE THIN FILMS

A THESIS SUBMITTED TO  
THE GRADUATE SCHOOL OF NATURAL AND APPLIED SCIENCES  
OF  
MIDDLE EAST TECHNICAL UNIVERSITY

BY  
BÜŞRA EKİM SARAÇ

IN PARTIAL FULFILLMENT OF THE REQUIREMENTS  
FOR  
THE DEGREE OF MASTER OF SCIENCE  
IN  
METALLURGICAL AND MATERIALS ENGINEERING

JANUARY, 2017



Approval of the thesis:

**STRUCTURAL AND OPTOELECTRONIC PROPERTIES OF SOL-GEL  
DERIVED NICKEL OXIDE THIN FILMS**

submitted by by **BÜŞRA EKİM SARAÇ** in partial fulfillment of the requirements for  
the degree of **Master of Science in Metallurgical and Materials Engineering**  
**Department, Middle East Technical University** by,

Prof. Dr. Gülbin Dural Ünver \_\_\_\_\_  
Dean, Graduate School of **Natural and Applied Sciences**

Prof. Dr. C. Hakan Gür \_\_\_\_\_  
Head of Department, **Metallurgical and Materials Engineering**

Prof. Dr. Caner DURUCAN \_\_\_\_\_  
Supervisor, **Metallurgical and Materials Eng. Dept., METU**

Assoc. Prof. Dr. H. Emrah ÜNALAN \_\_\_\_\_  
Co-Supervisor, **Metallurgical and Materials Eng. Dept., METU**

**Examining Committee Members:**

Prof. Dr. Kadri AYDINOL \_\_\_\_\_  
Metallurgical and Materials Engineering Dept., METU

Prof. Dr. Caner DURUCAN \_\_\_\_\_  
Metallurgical and Materials Engineering Dept., METU

Assoc. Prof. Dr. H. Emrah ÜNALAN \_\_\_\_\_  
Metallurgical and Materials Engineering Dept., METU

Assoc. Prof. Dr. Burcu AKATA KURÇ \_\_\_\_\_  
Micro and Nanotechnology, METU

Assoc. Prof. Dr. Ziya ESEN \_\_\_\_\_  
Materials Science and Engineering Dept., Çankaya University

**Date:** 18.01.2017

**I hereby declare that all information in this document has been obtained and presented in accordance with academic rules and ethical conduct. I also declare that, as required by these rules and conduct, I have fully cited and referenced all material and results that are not original to this work.**

Name, Last name: Būşra Ekim SARAÇ

Signature :

## **ABSTRACT**

### **STRUCTURAL AND OPTOELECTRONIC PROPERTIES OF SOL-GEL DERIVED NICKEL OXIDE THIN FILMS**

Saraç, Büşra Ekim

M.S., Department of Metallurgical and Materials Engineering

Supervisor: Prof. Dr. Caner DURUCAN

Co-supervisor: H. Emrah ÜNALAN

January 2017, 78 pages

Nanocrystalline nickel (II) oxide (NiO) thin films were deposited on glass substrate by spin coating of sol-gel derived solutions. Thin film formation behavior and microstructural / physical properties of the films were investigated as a function of controllable processing parameters, such as thin film thickness and post deposition heat treatment (annealing temperature) in the range of 400 – 500 °C. Microstructural, morphological and optoelectronic properties of NiO films was examined by scanning electron microscopy, atomic force microscopy, X-ray diffraction, UV-Vis spectroscopy, Raman spectroscopy, X-ray photoelectron spectroscopy, and temperature-dependent resistivity measurements. It was shown that microstructurally homogeneous and pristine film formation with controllable particle size of 10 – 30 nm can be achieved in a reproducible manner through the sol-gel processing route.

Sol-gel derived films of variable thickness in the range of 60 – 170 ( $\pm 5$  nm), exhibited a transparency of 80 % to 65 % in the visible range, negligible changing with annealing temperature. This work presents a parametric optimization approach of sol-gel deposition of NiO thin films and their optoelectronic characteristics.

**Keywords:** p-type transparent oxide thin films, nickel oxide, sol-gel, optoelectronic properties.

## ÖZ

### ŞEFFAF / YARI İLETKEN NİKEL OKSİT İNCE FİMLERİN SOL-JEL TEKNİĞİ İLE ÜRETİLMESİ

Saraç, Büşra Ekim

Yüksek Lisans, Metalurji ve Malzeme Mühendisliği Bölümü

Tez Yöneticisi: Prof. Dr. Caner DURUCAN

Ortak Tez Yöneticisi: Doç. Dr. H. Emrah ÜNALAN

Ocak 2017, 78 sayfa

Nanoparçacık yapıdaki nikel (II) oksit (NiO) ince filmler (kaplamalar) cam yüzeylere sol-jel tekniği kullanılarak döndürme yöntemiyle kaplanmıştır. Üretilen ince filmlerin oluşum davranışları, mikroyapısal ve fiziksel özellikleri ince film kalınlığına ve kaplama sonrası 400 – 500 °C arasındaki ısı işlem sıcaklığına (tavlama sıcaklığına) göre incelenmiştir. İnce filmlerin mikroyapısal, morfolojik ve optoelektronik özellikleri taramalı elektron mikroskobu, atomik güç mikroskobu, X-ışını kırınımı yöntemi, UV-görünür bölge spektroskopisi, Raman spektroskopisi, X-ışını fotoelektron spektroskopisi ve sıcaklığa bağlı direnç değişimi ölçümleriyle incelenmiştir. İnce filmlerin mikroyapısal olarak yüzeye homojen ve düzgün dağılan 10 – 30 nm arasındaki kristallenmiş nanoparçacıklardan oluştuğu ve sol-jel

yöntemiyle üretimin tekrarlanabilirliği gözlemlenmiştir. 60 - 170 nm ( $\pm$  5 nm) arasında farklı kalınlıklarda üretilen ince filmlerin, görünür bölgede % 80' den % 65'e kadar optik geçirgenliğinin olduğu gösterilmiştir. Bu çalışma, sol-jel yöntemiyle farklı parametreler doğrultusunda üretilen filmlerin mikroyapısal ve optoelektronik özelliklerindeki değişimi göstermektedir.

**Anahtar Kelimeler:** p-tipi şeffaf iletken oksitler, nikel oksit, sol-jel, optoelektronik özellikler

*To My Family*

## ACKNOWLEDGEMENTS

First and foremost, I would like to express the deepest appreciation to Dr. Caner Durucan for his support with friendly attitude. I also would like to thank Dr. H. Emrah Ünalın for his guidance throughout my thesis study.

I acknowledge support from The Scientific and Technological Research Council of Turkey (TUBITAK) BİDEB-2010-C-2014-3 program for the financial support.

I extend my sincere thanks to my labmates Barış Alkan, Özlem Altıntaş Yıldırım and Bersu Baştuğ from Materials Chemistry Laboratory. In addition, I would like to thank to my labmates Mete Batuhan Durukan, Sevim Polat, Ece Alpugan, İpek Bayraktar, Şahin Coşkun, Doğa Doğanay, Ayşegül Afal, Onur Türel, Alptekin Aydınlı, İtir Bakış Doğru, Doğançan Tigan, Pantea Aurang and Recep Yüksel from Nanomaterials & Devices Laboratory for their kind help and kindness.

I also would like to thank to Mustafacan Kutsal, Hazar Şeren, Bahadır Can Kocaoğlu, Murat Güneş, Berk Akbay, Utku Er, Mehmet Acun for their supports and friendships. I am thankful for Kerem Çağatay İçli for his help and comments during this study. I also appreciate his logistic and social supports. I would like to specially thank to all the technical staff of Metallurgical and Materials Engineering Department and METU Central Laboratory for their suggestions, help and comments during this study. In addition, I would like to thank to Arzu Film and its artists for keeping me company throughout all my undergraduate and graduate studies.

I would also want to express my gratitude for my lifelong friends Özge Ekici Demirel, Eda Kartal, Selin Cantürk, Zeynep Nilüfer Güven Öztürk and Burcu Taş for their unconditional friendship.

I am grateful to Deniz Olgu Devecioğlu for his patience and kindheartedness. I could not get through this study without his support. Words can never be enough to express my appreciation. He will be in my memory with joyful moments.

Lastly, I would like to thank to my mother, father and brother for their endless love, support and patience during my whole life. This thesis is dedicated to them.



## TABLE OF CONTENTS

<b>ABSTRACT.....</b>	<b>V</b>
<b>ÖZ.....</b>	<b>VII</b>
<b>ACKNOWLEDGEMENTS .....</b>	<b>X</b>
<b>TABLE OF CONTENTS .....</b>	<b>XIII</b>
<b>LIST OF TABLES .....</b>	<b>XVII</b>
<b>LIST OF FIGURES .....</b>	<b>XIX</b>
<b>1. INTRODUCTION .....</b>	<b>21</b>
<b>1.1. General Introduction and Rationale of the Thesis .....</b>	<b>21</b>
<b>1.2. Background Information and Literature Review .....</b>	<b>3</b>
1.2.1. Transparent Conductive Oxides (TCOs) .....	3
<b>1.3. NiO Thin Films.....</b>	<b>8</b>
1.3.1. Electrical Properties of NiO Thin Films .....	8
1.3.2. Optical Properties of NiO Thin Films.....	10
<b>1.4. Applications of NiO Thin Films.....</b>	<b>11</b>
1.4.1. Organic Light Emitting Diodes (OLEDs).....	11

1.4.2. Organic Photovoltaic Cells .....	13
1.4.3. Thin Film Transistors (TFTs) .....	14
1.4.4. Electrochromic Devices (ECDs).....	15
<b>1.5. Production Techniques for NiO Thin Films.....</b>	<b>18</b>
1.5.1. Pulsed Laser Deposition (PLD) .....	18
1.5.2. Sputtering.....	19
1.5.3. Chemical Vapor Deposition.....	20
1.5.4. Chemical Spray Pyrolysis (CSP).....	21
1.5.5. Sol-gel Processing.....	22
<b>1.6. Sol-gel Based Coating Techniques.....</b>	<b>24</b>
1.6.1. Spray Coating.....	24
1.6.2. Dip Coating.....	25
1.6.3. Spin Coating .....	26
<b>1.7. Preparation of NiO Coating Sol: Processing Details .....</b>	<b>27</b>
1.7.1. Nickel Precursors.....	27
1.7.2. Solvents and Stabilizers .....	29
<b>1.8. Parameters Affecting the Quality of Sol-gel Deposited NiO films .....</b>	<b>30</b>
1.8.1. Annealing Temperature .....	31
1.8.2. Thin Film Thickness .....	32
<b>1.9. Objective of the Thesis.....</b>	<b>35</b>
<b>2. MATERIALS AND METHODS .....</b>	<b>37</b>
<b>2.1. Materials .....</b>	<b>37</b>
<b>2.2. Experimental Procedure .....</b>	<b>37</b>
2.2.1. Cleaning Procedure of Glass Substrates .....	37

2.2.2. Preparation of Coating Sol.....	38
2.2.3. Deposition of NiO Thin Films .....	39
<b>2.3. Materials Characterization .....</b>	<b>40</b>
2.3.1. X-ray Diffraction (XRD) .....	41
2.3.2. Atomic Force Microscopy (AFM) .....	41
2.3.3. Scanning Electron Microscopy (SEM) .....	41
2.3.4. X-ray Photoelectron Spectroscopy (XPS) .....	41
2.3.5. Raman Spectroscopy.....	42
2.3.6. UV-Vis Spectrophotometry .....	42
2.3.7. Temperature-dependent Resistivity Measurements .....	42
<b>3. RESULTS AND DISCUSSION .....</b>	<b>43</b>
<b>3.1. Structural and Morphological Properties of NiO Thin Films .....</b>	<b>43</b>
3.1.1. XRD Analyses .....	43
3.1.2. AFM Analyses .....	45
3.1.3. SEM Analyses.....	46
3.1.4. Raman Spectroscopy.....	50
3.1.5. XPS Analyses.....	52
<b>3.2. Optical Properties of NiO Thin Films: UV-Vis Analyses.....</b>	<b>55</b>
<b>3.3. Electrical Properties of NiO Thin Films: Temperature-dependent Resistivity Measurements.....</b>	<b>59</b>
<b>4. CONCLUSIONS .....</b>	<b>63</b>
<b>5. REFERENCES.....</b>	<b>65</b>



## LIST OF TABLES

### TABLES

<b>Table 1.1.</b> Applications of representative metal oxide materials in microelectronics, including transparent conducting oxides, diodes, random access memories, solar cells and organic photovoltaics .....	4
<b>Table 1.2.</b> List of various p-type TCOs with their optical and electrical properties...	5
<b>Table 2.1.</b> List of chemicals used in NiO sol preparation .....	37
<b>Table 3.1.</b> Average particle size and thickness of NiO films determined from the SEM micrographs using the instrument (FEI Quanta 400 FEG/C) image processing software.....	50



## LIST OF FIGURES

### FIGURES

<b>Figure 1.1.</b> Figure showing the computation of the elements which exhibit the lowest electron effective masses in their respective binary oxides .....	6
<b>Figure 1.2.</b> Effect of ITO film thickness on PET substrate on optical transmission and resistivity.....	7
<b>Figure 1.3.</b> Rock salt crystal structure of NiO .....	8
<b>Figure 1.4.</b> The schematic cross-section of OLED .....	13
<b>Figure 1.5.</b> Device architecture of a typical bulk heterojunction solar cell with hole transport layer as PEDOT:PSS and NiO and energy band diagram of the corresponding layers .....	14
<b>Figure 1.6.</b> Schematic cross-section of solution-processed NiO based TFT with a bottom-gate bottom-contact structure. NiO <sub>x</sub> based active layers and the AlO <sub>x</sub> gate insulator are deposited by spin coating.....	15
<b>Figure 1.7.</b> The fundamental structure of ECDs .....	17
<b>Figure 1.8.</b> Schematic view of PLD system.....	19
<b>Figure 1.9.</b> The general simplified scheme for spray pyrolysis .....	22
<b>Figure 1.10.</b> Effect of pH on structure of gel.....	23
<b>Figure 1.11.</b> The schematic of sol-gel method.....	24
<b>Figure 1.12.</b> Schematic illustration of dip coating technique. ....	26
<b>Figure 1.13.</b> Schematic illustration of spin coating process .....	27
<b>Figure 1.14.</b> Effect of number of layers on thickness of NiO thin films. ....	33
<b>Figure 1.15.</b> Variation of the grain size with the number of layers constituting NiO films .....	34

<b>Figure 1.16.</b> Effect of number of layers on the optical band gap of NiO films .....	35
<b>Figure 2.1.</b> Processing details for preparation of NiO coating sol.....	39
<b>Figure 2.2.</b> Experimental procedure for fabrication of NiO thin films .....	40
<b>Figure 3.1.</b> XRD diffractograms of 15 times coated NiO films annealed in air at different temperatures.....	44
<b>Figure 3.2.</b> AFM images of 10 times coated NiO films annealed at 400 (a,b), 450 (c,d) and 500 °C (e,f).....	45
<b>Figure 3.3.</b> Top view SEM micrographs 60 nm thick NiO films annealed in air at (a) 400, (b) 450 and (c) 500 °C at the same magnification. (d) Cross-sectional SEM image of 60 nm thick NiO film annealed at 400 °C. ....	47
<b>Figure 3.4.</b> Top view SEM micrographs 110 nm thick NiO films annealed in air at (a) 400, (b) 450 and (c) 500 °C at the same magnification. (d) Cross-sectional SEM image of 60 nm thick NiO film annealed at 450 °C. ....	48
<b>Figure 3.5.</b> Top view SEM micrographs 170 nm thick NiO films annealed in air at (a) 400, (b) 450 and (c) 500 °C at the same magnification. (d) Cross-sectional SEM image of 170 nm thick NiO film annealed at 500 °C. ....	49
<b>Figure 3.6.</b> Raman spectra of 170 nm thick NiO films annealed at different temperatures.....	51
<b>Figure 3.7.</b> Regional XPS spectra for (a) Ni 2p and (b) O 1s core levels of the NiO thin films annealed in air at different temperatures. ....	54
<b>Figure 3.8.</b> Optical transmission spectra of (a) 60, (b) 110 and (c) 170 nm thick NiO films annealed at 400, 450 and 500 °C. ....	57
<b>Figure 3.9.</b> Optical band gap of (a) 60, (b) 110 and (c) 170 nm thick NiO films annealed at 400, 450 and 500 °C. ....	58
<b>Figure 3.10.</b> Temperature-dependent resistivity plots and the corresponding activation energies (in eV) for 170 nm thick NiO film annealed at (a) 400, (b) 450 and (c) 500 °C.....	60

## CHAPTER 1

### INTRODUCTION

#### 1.1. General Introduction and Rationale of the Thesis

Metal oxides in various morphologies, shapes and sizes have received extensive attention due to their unique and tunable chemical and physical properties. They are essential materials for electronic and optoelectronic applications. On the other hand, it is known that reduction of particle size of a material to nanometer scale changes the properties of the matter and impart intriguingly new properties. Therefore, nanostructured metal oxides are promising materials to explore future electronics.

NiO is a well known wide band gap (3.6-4.0 eV) semiconductor possessing p-type conductivity. It has been widely used in gas sensing [1], catalysis [2], electrochromic [3] and optoelectronic applications. Most of such electronic applications require thin, homogeneous and non-porous layers in order to exhibit low resistance and high carrier diffusion length. NiO thin films have been deposited onto glass substrates using various techniques like magnetron sputtering [4], pulsed laser deposition [5], chemical vapor deposition [6] and sol-gel process [7]. Among them, sol-gel method is promising with its low cost, simple equipment requirement and scalability. In addition, it allows the reproducible deposition of high purity thin films, practiced by spray, dip or spin coating techniques for the fabrication of thin film. Spin coating is a versatile and widely used technique for the fabrication of thin films on various planar substrates.

Spin coated NiO thin films have been deposited from aqueous solutions of nickel salts including nickel nitrate [1], sulphate [8], chloride [9] or organic precursors like acetate [10], nickel diacetate [11] and nickel 2-ethylhexonate [12] with the addition of proper agents or pH regulators. Nickel acetate is one of the most preferred nickel sources used in sol-gel based routes due to its relatively low decomposition temperature [13].

Structural, optical and electrical properties of NiO thin films deposited on different substrates have been studied with respect to annealing temperature for a chosen thickness [10,14]; whereas, the studies investigating the effect of thin film thickness on such properties are limited [15]. Optoelectronic devices like light emitting diodes, organic light emitting diodes employ NiO thin films as hole injection layers, while solar cells employ them as hole transport layers [14,16]. Compared to organic counterparts like poly(3,4-ethylenedioxythiophene)polystyrene sulfonate or poly(3-hexylthiophene-2,5-diyl), inorganic NiO layers show excellent performance by means of device stability and efficiency [16,17]. Abundance of NiO is another advantage among its polymeric counterparts. Thin NiO layers used in these devices are expected to simultaneously exhibit sufficient electronic conduction, visible light transmission and hole transport ability when deposited in a thickness range of 50 – 100 nm [14, 18]. Deposition and formation of homogeneous, dense and crack free NiO films in this thickness requirement is of critically important for proper device function.

In this study, a parametric investigation on the sol-gel deposition of NiO thin films were conducted with a special emphasize on reproducible controllability of thin film thickness. The effect of both film thickness and post deposition heat treatment (annealing) temperature on the morphological and optoelectronic properties of NiO thin films have been reported and discussed.

## **1.2. Background Information and Literature Review**

### **1.2.1. Transparent Conductive Oxides (TCOs)**

Transparent conducting oxides (TCOs) are degenerately doped wide band gap semiconducting metal oxides offering good electrical conductivity with high optical transparency to visible light. Most TCOs are binary or ternary compounds, having one or two metallic elements. By nature, number and atomic arrangements of metal cations in crystalline/amorphous oxide configuration, morphology and intrinsic/extrinsic defects constitute the electrical and optical properties of TCOs. In 1907, the first TCO thin film of CdO was reported by Badeker [19]. CdO thin film was firstly deposited by thermally oxidizing a vacuum sputtered film of cadmium. Although, CdO possesses high electron mobility due to its low effective electron mass, serious toxicity doubts about CdO restrict its usage. Then, ZnO, SnO<sub>2</sub>, In<sub>2</sub>O<sub>3</sub> and their derivatives were also introduced as TCOs [20].

In today's technology, Al doped ZnO (AZO), tin doped In<sub>2</sub>O<sub>3</sub> (ITO) and fluorine/antimony doped SnO<sub>2</sub> (FTO/ATO) are commercially available and widely utilized in industrial applications such as photovoltaic cells [21], display devices [22], functional glasses [23], light emitting diodes [24] and electrochromic devices [25]. Representative device applications of metal oxides are given in Table 1.1. Not only the optical and electrical properties, but also the environmental stability, compatibility with the other materials and substrates used in device structure are essential factors for choosing suitable TCOs in device applications. Additionally, costs of the raw materials and deposition process are the other key parameters for utilization of the TCO materials.

**Table 1.1.** Applications of representative metal oxide materials in microelectronics, including transparent conducting oxides, diodes, random access memories, solar cells and organic photovoltaics, adapted from [26].

Application	Metal Oxide	Deposition Technique	Processing Temperature (°C)
<b>p-n junction</b> Diodes Sensors  Solar Cells	CuCrO <sub>2</sub> :Mg-ZnO WO <sub>3</sub> -SnO <sub>2</sub> ZnO-SnO <sub>2</sub> ZnO-SnO <sub>2</sub> Ga <sub>2</sub> O <sub>3</sub> -Cu <sub>2</sub> O Cu <sub>2</sub> O-TiO <sub>2</sub> -ZnO (nanowire)	PLD Sol-gel Sol-gel PECVD PLD Vapour + ALD	RT (laser annealing) 200 300 350 RT 1,140 (HP O <sub>2</sub> )
<b>Random access memories</b>	Cu <sub>x</sub> O	ECP	NA
<b>Transparent conducting oxides</b>	ZrO <sub>2</sub> NiO ITO AZO IZO GZO ZITO	Sol-gel Sputtering Sputtering Sputtering Sputtering Sputtering Sputtering	600 300 RT RT RT RT RT
<b>Organic photovoltaics</b> Electrode  Interfacial layer	ITO InCdO-ITO ZITO MoO <sub>3</sub> V <sub>2</sub> O <sub>5</sub> ZnO NiO TiO <sub>x</sub>	Commercial IAD PLD Thermal evaporated Thermal evaporated Sol-gel PLD Sol-gel	NA RT RT NA NA 150 RT 150

Most of the conventional TCOs are n-type and commercial ones are also available, but the current p-type TCOs have not yet employed in practical/commercial industrial applications. Additionally, various possible applications of n-type TCOs are also incomplete due to the lack of their p-type counterparts. The recent studies on TCO technology have focused on developing novel p-type TCOs to deposit them as thin films. The most common p-type TCOs reported in literature are listed in Table 1.2.

High performance p-type TCOs would promise the improvement of optoelectronic devices and transparent electronic applications by the construction of p-n heterojunction structures accompanying common n-type TCOs.

**Table 1.2.** List of various p-type TCOs with their optical and electrical properties, adapted from [27].

Materials	Structure	Growth methods	D (nm)	T (%)	E <sub>opt</sub> (eV)	σ (S cm <sup>-1</sup> )	μ (cm <sup>2</sup> V <sup>-1</sup> s <sup>-1</sup> )
Sn:In <sub>2</sub> O <sub>3</sub> (ITO)	Bixbyite	Sputtering	115	85	3.7	5900	30
Cu <sub>2</sub> O	Cubic	PLD	650	---	2.17	0.014	90
CuBO <sub>2</sub>	Delafossite	PLD	200	75	4.5	1.65	100
CuAlO <sub>2</sub>	Delafossite	PLD	500	28	3.5	0.95	10.4
CuAlO <sub>2</sub>	Delafossite	PLD	230	70	3.5	0.34	0.13
CuCr <sub>0.95</sub> Mg <sub>0.05</sub> O <sub>2</sub>	Delafossite	PLD	250	30	3.1	220	---
CuGaO <sub>2</sub>	Delafossite	Sputtering	300	80	3.6	0.02	0.23
CuScO <sub>2+x</sub>	Delafossite	PLD	110	40	3.7	15	---
CuIn <sub>0.93</sub> Ca <sub>0.03</sub> O <sub>2</sub>	Delafossite	Sputtering	100	40	3.7	0.006	---
CuY <sub>1-x</sub> Ca <sub>x</sub> O <sub>2</sub>	Delafossite	PLD	100	41	3.5	1	---
SrCu <sub>2</sub> O <sub>2</sub>	Tetragonal	Sputtering	120	80	3.3	0.048	---
La <sub>0.97</sub> Sr <sub>0.03</sub> CuOS	Tetragonal	PLD	150	60	3.1	20	---
La <sub>0.8</sub> Mg <sub>0.2</sub> CuOse	Tetragonal	Sputtering	40	---	2.8	910	3.5
ZnRh <sub>2</sub> O <sub>4</sub>	Spinel	PLD	100-300	55	2.74	2.75	---
ZnIr <sub>2</sub> O <sub>4</sub>	Spinel	PLD	100-300	61	2.97	3.39	---
Mg <sub>x</sub> Cr <sub>2-x</sub> O <sub>3</sub>	Corundum	Solution	150	65	3.3	0.33	---
La <sub>0.75</sub> Sr <sub>0.25</sub> CrO <sub>3</sub>	Perovskite	MBE	80	55	4.6	15	0.03
La <sub>0.50</sub> Sr <sub>0.50</sub> CrO <sub>3</sub>	Perovskite	MBE	50	43	4.6	56	0.04
SnO	Litharge	PLD	20	---	2.8	0.1	2.4
SnO	Litharge	Sputtering	200	0.85	2.8	0.77	4.8
Ba <sub>2</sub> BiTaO <sub>6</sub>	Perovskite	PLD	120	90	4.5	0.005	30
Li:NiO	Rocksalt	Sputtering	118	30	3.4	7.1	---

The electrical conduction mechanism of TCOs can be explained by the physics of semiconductors. Concentration ( $n$ ) and the mobility ( $\mu$ ) of the charge carriers determines the electrical conductivity ( $\sigma$ ) of TCO thin films by the relation of  $\sigma = ne\mu$  where  $e$  is the charge of the elementary particles. The parameter  $n$  is determined by the intrinsic mobile carrier generation of charge carriers (electrons or holes depending n-type or p-type conduction mechanism, respectively) due to dopants or defects. According to the expression of  $\mu = e\tau/m^*$ , free carrier relaxation time  $\tau$  directly and the effective mass of carriers  $m^*$  inversely depend on the mobility of carriers  $\mu$ .  $\tau$  is mainly

effected by extrinsic elements like grain boundaries, vacancies or ionized dopants. The  $m^*$  is a tensor with the components of energy ( $\varepsilon$ ) and momentum ( $k$ ) vectors. Therefore, curvature of conduction band minimum or valence band maximum in structure leads to small  $m^*$  and then high  $\mu$ . Conductivities of TCOs can be adjusted by selection of suitable dopant element with respect to their effective mass of carriers. The electron effective mass of the elements in their corresponding binary oxides is given in Figure 1.1.

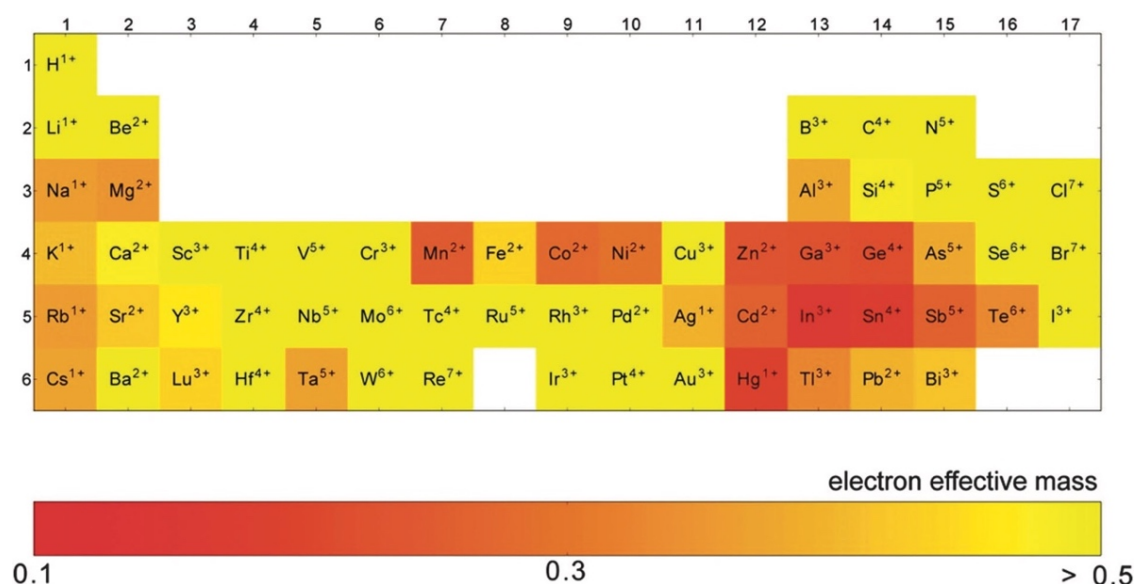


**Figure 1.1.** Figure showing the computation of the elements which exhibit the lowest electron effective masses in their respective binary oxides [28].

On the other hand,  $\mu$  is a limited parameter. If there is large separation between conduction band minimum and valence band maximum ( $\sim$ above 3eV), conduction band could not be occupied at room temperature thermally ( $kT \sim 0.03$  eV, where  $k$  is Boltzmann's constant). Thus, stoichiometric crystalline TCOs behave as excellent insulators [29]. However, visible range of the spectrum is between 1.8 and 3.1 eV. Therefore, for transparency to the visible portion of the spectrum, the distance between conduction band minimum and valence band maximum of TCOs should be in this

energy range. This contradiction about the value of band gap is resolved by doping. It was observed that increase in the electrical conductivity without loss of optical transparency can be achieved by doping of TCOs [20].

However, the large concentration of charge carriers, leads to reduction in optical transparency and conductivity, so film thickness and doping rate should be considered in designation of TCOs. Effect of thin film thickness on the optical transmission and electrical resistivity of film is shown in Figure 1.2.

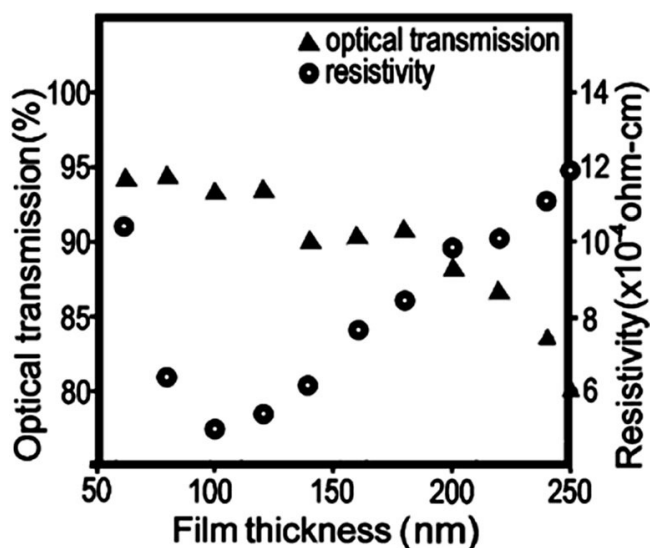


**Figure 1.2.** Effect of ITO film thickness on PET substrate on optical transmission and resistivity [28].

An increase in film thickness and doping amount enhances the electrical conductivity up to some extent. Free charge carrier absorption become an essential mechanism in case of a high doping amount by means of optical properties. Excess amount of doping and high carrier/defect concentration due to increase in thickness enhance the density of defect sites (dopant). Therefore, characteristics of dopants gradually become dominant by scattering effect of these sites. The reductions of the mean free path of

charge carriers and then, relaxation time of free carriers decrease the conductivity of thin films [28]. Excess amount of doping and increase in thickness cause the shift of donor/acceptor level, by getting them closer to conduction band/valence band. Thus, optical band gap becomes wider, causing a change in the optical transparency of the resultant thin film [28]. Additionally, high concentration of charge carriers can cause imperfections in optical absorption at IR, visible and/or UV wavelengths due to the dominant free charge carrier absorption process [30].

### 1.3. NiO Thin Films

NiO has a rock salt type crystal structure presented in Figure 1.3 with the band gap around 3.4 - 4.0 eV and it is the first reported p-type TCO thin film deposited using RF magnetron sputtering by Sato et al. [31]. Conductivity of these films were nearly  $7.1 \text{ S cm}^{-1}$  and optical transparencies to visible range were about 40%.

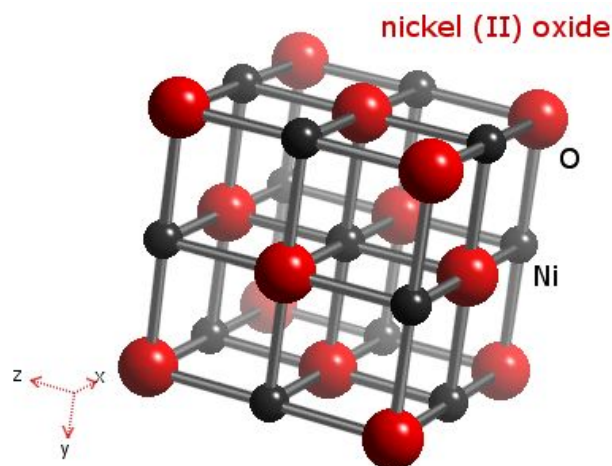


**Figure 1.3.** Rock salt crystal structure of NiO, retrieved from [32].

#### 1.3.1. Electrical Properties of NiO Thin Films

Pure stoichiometric NiO is an excellent insulator. Conduction mechanism of NiO has not clearly explained yet, so there is no common agreement about its electrical properties [33]. Firstly, it was believed that stoichiometric NiO is Mott insulator [34]. Then, it is corrected that it behaves as Mott-Hubbard type insulator [35]; however,

when it is oxidized, it becomes a p-type conductor [36]. However, my conflicting results reveal that conduction mechanism and electronic structure of NiO is quite complex than that has been proposed [37, 38, 4, 39, 40, 41]. The conduction mechanism of NiO has been explained as percolative [37], small polaronic [40] and grain boundary controlled [42, 38, 41]. Similarly, the conflictive results about Hall conductivity of NiO has been also reported [41, 43]. The highest p-type Hall mobility of NiO thin films deposited using RF magnetron sputtering was reported as  $28.56 \text{ cm}^2 \text{ V}^{-1} \text{ s}^{-1}$  by Chen et al [44]. Nevertheless, one can realize that measuring the Hall mobility is not reliable and trivial due to very low mobility values ( $\ll 1 \text{ cm}^2 \text{ V}^{-1} \text{ s}^{-1}$ ) of  $\text{Ni}_{1-x}\text{O}$  and  $\text{Li}_x\text{Ni}_{1-x}\text{O}$  thin films. Although it has quite low conductivity, NiO is one of the most widely preferred p-type TCO in device applications [14, 26].

The huge differences between the studies about the electrical properties of NiO can be due to non-uniform composition of samples, inadvertent doping, or grain boundaries. Additionally, accurate measuring of the oxygen amount in the structure of the final composition is quite difficult, which leads to inconsistent results. It has been also notified that oxidized NiO (such as  $\text{Ni}_2\text{O}_3$  or introduction of Ni vacancies) is located at the grain boundaries of polycrystalline structure resulting in new pathways for additional conduction mechanism through grain boundaries [42, 38, 41]. Moreover, there are some reports reveal that thermal annealing, electron and ion impact also have significant influence on defect formation and concentration. These combined difficulties and conditions cause the inconsistencies and confusions on the reported results.

According to the latest studies, p-type conduction in NiO is provided by hole states induced through Ni vacancies in case of oxygen-rich environments [27]. The another way to enhance the conductivity of NiO is doping. Although there are many dopants reported in literature such as Ga, Cr, In, Mg, Ag, Na and Zn [45, 46], the most common practice is doping NiO with  $\text{Li}^+$  sites ( $\text{Li}_x\text{Ni}_{1-x}\text{O}$ ) [47]. It has been concluded that,  $\text{Li}^+$  ions substitute Ni sites and crystal structure does not change if the doping is lower than

0.25 atomic ratio.  $\text{Li}^+$  ions constitute hole states at the top of valence band; however, the nature of hole state ( $\text{Ni}^{3+}$  or O) is a controversial issue due to strong electron correlation in the structure [48]. The significant reason of the conductivity limitation of  $\text{Ni}_{1-x}\text{O}$  or  $\text{Li}_x\text{Ni}_{1-x}\text{O}$  is this strong electron correlation due to 3d orbitals. In literature, the highest conductivity values of  $\text{Ni}_{1-x}\text{O}$  and  $\text{Li}_x\text{Ni}_{1-x}\text{O}$  have been reported as  $7.1 \text{ S cm}^{-1}$  [47]. Additionally, the temperature-dependent resistivity studies reveal that conductivity of  $\text{Ni}_{1-x}\text{O}$  and  $\text{Li}_x\text{Ni}_{1-x}\text{O}$  obey Arrhenius relation. However, it is not clear that the conduction mechanism is whether through small polarons or band like [49, 42, 50].

### 1.3.2. Optical Properties of NiO Thin Films

NiO is green due to strong absorption in violet (2.75 – 2.95 eV) and red (1.75 eV). In case of an excess oxygen, namely Ni is oxidized by directly oxygen or doping with  $\text{Li}^+$ , high absorption coefficient of the green range (1.75 – 2.75 eV) is expanded and NiO appears as black [51]. Band gap of NiO thin films changes with the deposition technique in between 3.4 and 4.3 eV.

To understand the electronic structure of NiO, various optical experiments has been carried out such as photoemission or inverse photoemission studies [33, 39, 52]. Theoretical calculations about optical spectra have also been reported [53]. There are some significant points about conduction band, valence band and optical band gap of NiO to be noticed:

- Ni 3d states dominates the conspicuous structure at valence band edge [39, 52].
- Ni 4s is located at the conspicuous structure of conduction band edge, but the structure on the small shoulder ( $(E_c - E) \sim 0.8 \text{ eV}$ ) is detected and considered as localized Ni states [54].
- The gap of band structure is clean due to its nature [39]; however, mid-gap structure is quite sensitive susceptible to thin film deposition and defects [39, 54].

#### **1.4. Applications of NiO Thin Films**

Nanocrystalline NiO thin films are attractive materials due to their excellent durability, chemical stability, controllable conductivity with high transparency and catalytic properties. Additionally, NiO is quite compatible to be incorporated with the wide range of n-type TCOs due to its rock salt structure resulting in ease of lattice matching [27].

Transparent conducting NiO films are employed in wide range range of device applications, such as organic light emitting diodes (OLEDs), photovoltaic devices, thin film transistors (TFT), electrochromic devices and gas sensors.

##### **1.4.1. Organic Light Emitting Diodes (OLEDs)**

Organic light emitting diodes (OLEDs) are optoelectronic devices which emit light from the emissive electroluminescent layer composed of an organic compound when electrical current is passed. OLEDs were invented in 1987 [55] and now they are commercially used in wide-range applications, such as small screens for mobile phones, portable digital audio players, televisions for residential light.

The multilayer OLEDs are thin film devices consisting basically organic emitting layer and hole transporting layer embedded between anode and cathode electrodes. The top electrode is generally highly reflecting whereas the bottom electrode has high transparency thin film deposited onto suitable transparent substrate. Simply, voltage is applied between anode and cathode electrodes. The holes are injected from cathode and electrons from the anode electrode by the electric current. The injected charges come together and recombine in emissive layer. Photons are created, so light is emitted, in a frequency corresponding to the energy gap between conduction band and valence band of this emissive layer.

Highly efficient OLEDs are generally fabricated using thermal evaporation, but this technique has some restrictions in manufacturing such as high processing cost and lack of ability to deposit onto large areas. On the other hand, solution-processed OLEDs

offer low cost and large area applications on flexible substrates. Although, low efficiency is often a problem for solution-based processing, this challenge can be eliminated by charge blocking layers. However, solution-based techniques limit the deposition of multilayer structures due to dissolving or damaging the subsequent layer by its solvent [56]. There are many reports on solution-based OLEDs using poly(3,4-ethylenedioxythiophene): poly(sterene sulfonate) (PEDOT:PSS) as hole injection layer by spin coating [57]. However, PEDOT:PSS is not able to effectively block electrons and excitons from emissive layer. Moreover, acidic nature of PEDOT:PSS can cause device instability [56]. Hence, a multilayer OLED usually requires a hole transporting layer for effective blocking of both electrons and excitons. Numerous organic hole transport materials have been also synthesized and experienced in OLEDs. However, most of them are not compatible with solution-based processing due to dissolving or washing away by the solvents of subsequent deposited layer.

Although, cross-linkable organic materials have been also tested as hole transport layer in OLEDs [58, 16], low efficiency has been observed due to low mobility of holes resulting the porous morphology of the films leading to reduction of cross-linking. Therefore, NiO is an alternative inorganic p-type semiconducting thin film as hole transporting and injection layer instead of organic molecules. NiO exhibits excellent hole selectivity, electron blocking capability and large ionization potential with high optical transparency. There are several reports on utilizing of NiO in OLEDs using sputtering [59], thermal evaporation [60] and most commonly solution-based processing [56]. The schematic structure of OLED with NiO hole transport/injection layer is depicted in Figure 1.4.

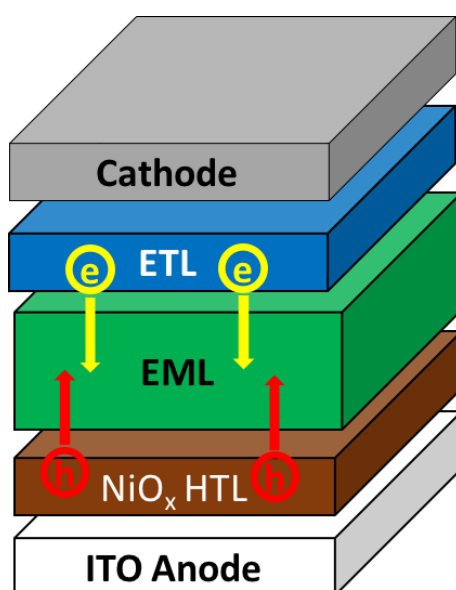


**Figure 1.4.** The schematic cross-section of OLED, adapted from [56].

#### 1.4.2. Organic Photovoltaic Cells

Photovoltaic (PV) cells employ the semiconducting materials to convert the light into electricity when exposed to light. Dye-sensitized solar cells (DSSC), organic solar cells and amorphous solar cells are commercially manufactured photovoltaics.

Organic photovoltaics (OPVs) employing organic molecules for light absorption and excitons formation also require electron and hole blocking layers in order to efficiently extract charges and reduce recombination rates. In such devices active layers (absorber) are stacked between hole transport and electron transport layers as depicted in Figure 1.5. In OPVs, PEDOT:PSS is mostly preferred efficient organic hole transport layer with a work function of 5.2 eV. However, a considerable amount of studies on the disadvantages of PEDOT:PSS have been reported [61, 62, 63]. Besides PEDOT:PSS is an organic molecule possessing high tendency to degrade in presence of water and sunlight which limit long term usage in PV device applications. All these problems cause the instability, degradation and low device performance.

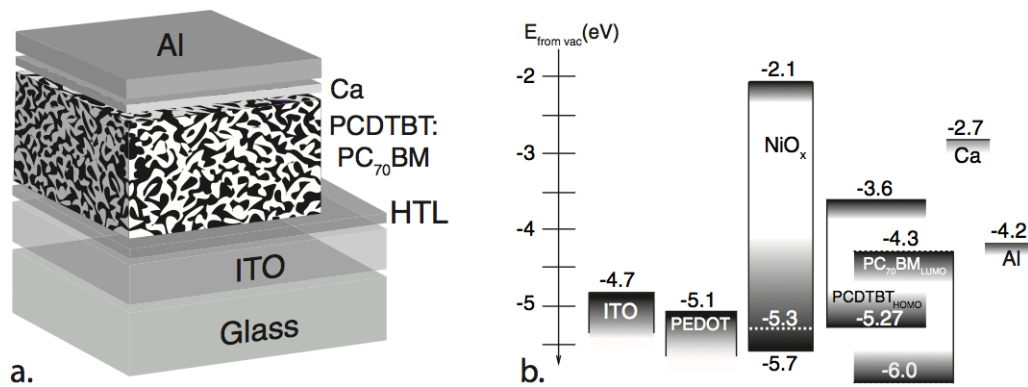


**Figure 1.5.** Device architecture of a typical bulk heterojunction solar cell with hole transport layer as PEDOT:PSS and NiO and energy band diagram of the corresponding layers [64].

On the other hand, NiO is a stable and robust ceramic material compared to organic PEDOT:PSS. Valence band maximum and work function of NiO are similar to that of PEDOT:PSS and NiO has been extensively utilized in wide range of OPVs as a hole transport/injection layer [14, 5, 65, 64, 66]. NiO has a wide band gap and deep valence band.

### 1.4.3. Thin Film Transistors (TFTs)

Thin film transistors (TFTs) take commercially place in today's technology, such as flat panel displays, smart phones and computers. These devices facilitate the advancing of video system technology by enabling the large dimension displays. They are most commonly utilized as the pixel switching components in flat panel displays. Additionally, this technology finds several applications apart from the display technologies, such as X-Ray detection [67], microelectronic devices (memories) [68], chemical sensors [69] and bio-chemical sensors [70].

TFTs are kind of field effect transistors principally containing three terminals (source, gate and drain) and including semiconducting, conducting and dielectric layers. The

semiconducting material is located between source and drain terminals; whereas, the dielectric one is placed between the semiconducting material and the gate. The working principle is to regulate the electric current between drain/source electrodes by change in the potential between gate/source, producing free charge accumulation between dielectric and semiconductor layer [71].

TFTs can be fabricated in different structures depending on arrangement of layers determined by the deposition process, post-processing heat treatments or amount of lithographic masks employed. Most common TFT structures are staggered bottom-gate, coplanar bottom-gate, staggered top-gate and coplanar top-gate.

NiO is promising material to fabricate low cost p-type oxide TFTs. Solution-based processing techniques are rather attractive than vacuum-based processes due to their simplicity, low cost and high quality films. Solution-processed NiO based p-type TFTs have been reported many times [72, 73, 74]. The schematic representation of cross sectional solution-processed NiO based p-type TFT structure is provided in Figure 1.6.

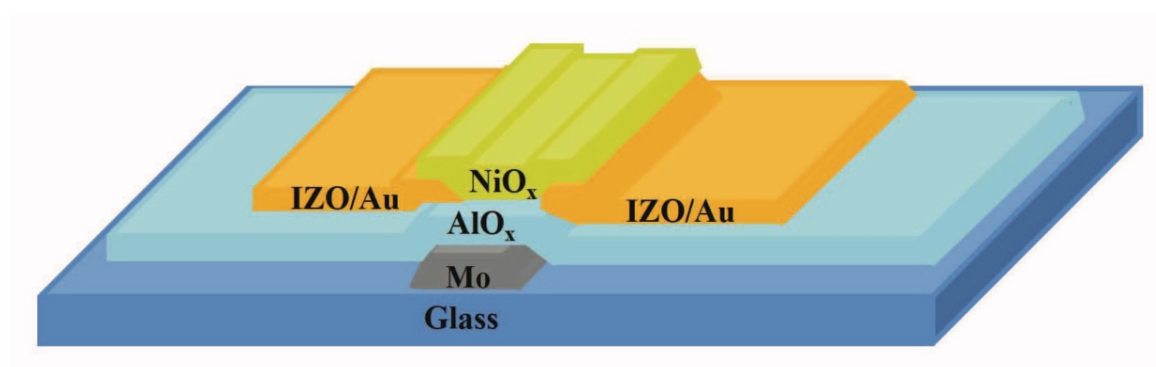


**Figure 1.6.** Schematic cross-section of solution-processed NiO based TFT with a bottom-gate bottom-contact structure. NiO<sub>x</sub> based active layers and the AlO<sub>x</sub> gate insulator are deposited by spin coating [72].

#### 1.4.4. Electrochromic Devices (ECDs)

Color of electrochromic materials can be changed, evocated or bleached when appropriate electrical potential is applied to initiate redox process. Electrochromic

devices (ECDs) or cells can be considered as some kind of rechargeable thin film batteries. ECDs including smart windows can modulate transmitted/reflected visible electromagnetic waves so they are utilized in sunroofs, filters, antiglare car mirrors, architectural applications and aerospace applications [75].

The generic structure of ECD is composed of a substrate that is coated with a transparent conducting material, the electrochromic coating, an electrolyte, an ion reservoir, an additional conductor and again a substrate [76]. The transparent conducting layer behaves as the electrode which provides the connection of device and external battery. Tin oxide ( $\text{SnO}_2$ ) or ITO thin films are mostly preferred materials coated on substrate as a transparent conductive electrode [77]. The electrochromic material is deposited onto transparent conductive substrate in thin film form. This electrochromic film is in contact with an ion conductive electrolyte whose other side is in contact with ion reservoir. The voltage is applied through this electrolyte and substrate coated with transparent conductive film. The electrical current drives the ions from reservoir into the electrochromic film over the electrolyte and injects the electrons from the conductive coating of the substrate. The optical characteristic of electrochromic layer is altered by the injected electrons due to their tendency to charge neutrality. The reverse voltage ejects the ions out from the reservoir and enables the leaving of electrons through the substrate; therefore, electrochromic material is converted to its original state. The schematic structure of ECDs is depicted in Figure 1.7.

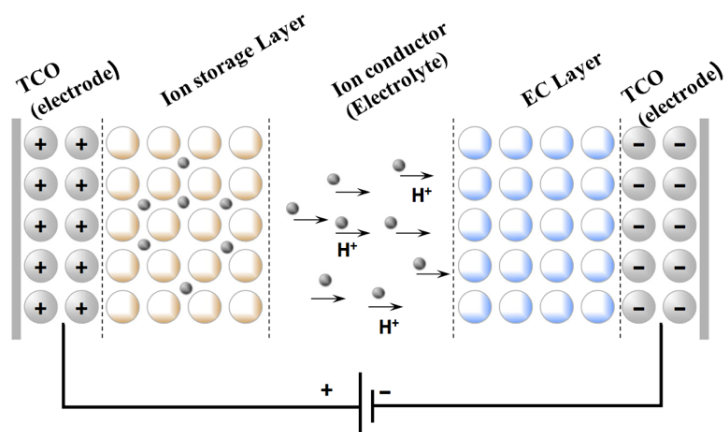


**Figure 1.7.** The fundamental structure of ECDs [17].

The electrochromic materials are divided into three groups.

- i. *Cathodically coloring* materials: These are colored in the reduced state and colorless in the oxidized state.



M is an alkali metal or hydrogen

- ii. *Anodically coloring* materials: These are colored in the oxidized state and colorless in the reduced state.



- iii. The electrochromic materials are colored in both oxidized and reduced states.

NiO is an anodically coloring inorganic material. In oxidized state, the color of NiO turns to dark bronze [76]. A considerable amount of studies has been recently reported on NiO as a counter electrode for NiO/ WO<sub>3</sub> electrochromic applications [17, 78]. It has not been clearly understood yet that the coloration mechanism of NiO is due to whether injection of hydroxyl or lithium ions, or extraction of protons [79].

## 1.5. Production Techniques for NiO Thin Films

### 1.5.1. Pulsed Laser Deposition (PLD)

Pulsed laser deposition (PLD) technique which is one of the physical vapor deposition methods offers to obtain high quality thin films with fine stoichiometry control. High purity and morphologically quite uniform NiO films can be deposited on different substrates such as Ni foil [80], quartz [81] or glass [66] and heteroepitaxial growth is also achievable by PLD technique [82]. PLD process is divided into three main steps: vaporization (ablation) of target materials, creation and transport of ablated plume and growth of the film on substrate. High power laser pulses focused by a series of lenses are used to ionize, melt and evaporate the material from the target surface. The fleeting bright plasma plume (consists of ions, electrons, other complex species etc.) that enlarges quickly away from the surface of a target is created by ablation process. Afterwards, thin film growth starts as a result of the subsequent collection, positioning and condensation of the ablated material on the surface of the substrate. The schematic illustration of PLD technique is given in Figure 1.8.

PLD is capable of fabricating complex/functional oxide thin films by transferring the stoichiometry from surface of the target to that of substrate, produce high purity multilayered thin films by using different targets without break the vacuum and control the film thickness, on the order of typically  $\sim 100 \text{ \AA}/\text{min}$ , in real time by tuning the laser. On the other hand, some species in the plume with high energy can lead to the re-sputtering and kind of defects on both the surface of substrate and growing layer. Since high power of laser is able to eject the macro/microparticles from the surface of the target, this can cause developing undesired properties of single or multiple layer growth [83]. Moreover, the poor energy output/input ratio and inconvenience in deposition onto large surfaces make PLD almost limited to research based technique.

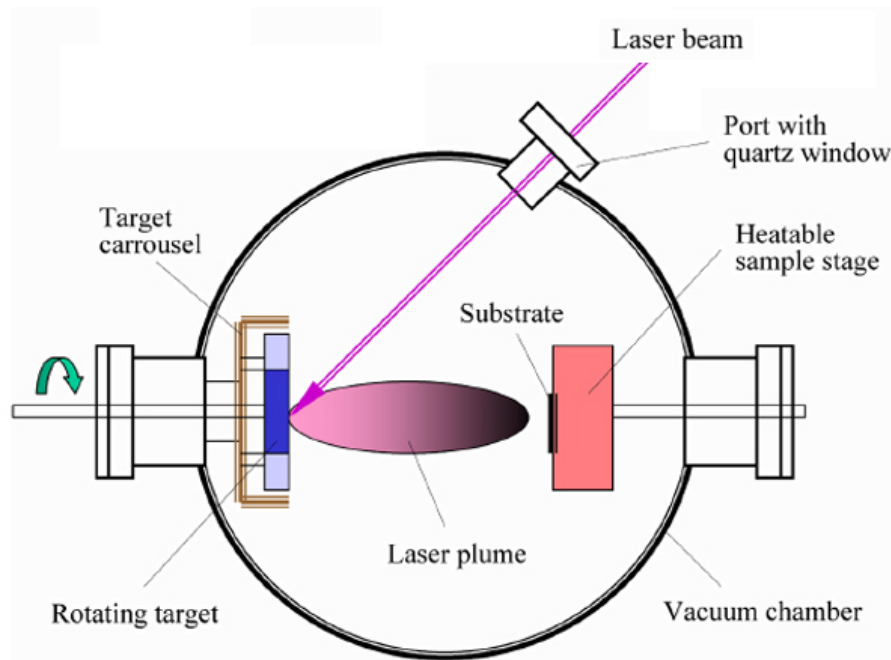


**Figure 1.8.** Schematic view of PLD system, retrieved from [84].

### 1.5.2. Sputtering

In sputtering method, atoms and/or molecules are ejected from the target or source material to be deposited on various substrates as a result of the bombardment via high energy particles (ions). Ion bombardment is basically a physical process resulting in a charged sputtered plasma; therefore, sputtering method is one of the physical deposition techniques. Substrate is placed in the vacuum chamber full of an inert gas (commonly Argon), then plasma is created onto substrate by negative charge applied to a target material. Free electrons are transported from the negatively charged target material through the plasma atmosphere which collides with the identically charged Argon gas atoms. Because of the negatively charged target, Argon atoms are converted to positively charged ions with high velocity. The particles from the target material crossing over the vacuum chamber with collisions reach the surface of the substrate and form the thin film. The number of atoms ejected from the target is called as sputter yield and depends on mass ratio of ions/target atoms, energy/angle of bombarding ions

and surface binding energy of target atoms [85]. This technique offers uniformity, reproducibility, control of stoichiometry and grain size, deposition of wide-variety of metals, composites or insulators with high deposition rates. Sputtering does not need the high temperatures; whereas, high pressure (1-100mtorr) is required for vacuum chamber. On the other hand, substrate damages, degradation of some materials (e.g. organics) can be observed and target can be heated by the ion bombardment.

Direct current (DC), pulse DC, radio frequency (RF), mid-frequency alternative current (MF-AC) and high power impulse magnetron sputtering (HIPIMS) are sputtering techniques classified by the power sources. Different types of sputtering methods such as magnetron, DC/RF reactive and ion beam sputtering are widely used for deposition of NiO thin films [86, 4, 87].

### **1.5.3. Chemical Vapor Deposition**

Chemical vapor deposition (CVD) technique uses gaseous phases of source material frequently diluted in carrier gases to form a thin film on desired substrate. Suitable one or more gasses produced from gasses (easiest), volatile liquids or sublimated solids, are delivered into reaction chamber at pressures usually of the order of 10 Pa. In reaction chamber, they reach to the surface of heated substrate and decompose thermally or react on or above the surface. On the growth sites, reactant gaseous species are diffused and condensed to form pristine solid film on the surface; however, the reactions without diffusion can cause the rough growth surface. By-products are produced during the chemical reactions on the surface and on the deposition of solid layer. Finally, by-products are desorbed and waste gasses are transported out of the reactor. Reaction temperature, melting point and stability at room temperature are critical parameters for source materials. The compatibility of substrate and source materials are also essential to carry out successive surface reactions and surface diffusion.

CVD covers large-scaled processes classified by operating pressure, physical characteristics, plasma methods etc. NiO thin films can be deposited using different types of CVD techniques, such as aerosol-assisted [6] and metal-organic CVD [88]. This technique offers high growth rates and purity, deposition of the materials that are hard to evaporate, reproducibility and fabrication of epitaxial films. On the other hand, high temperature requirement, complexity of the production process and toxic/corrosive gasses are the drawbacks of this technique.

#### **1.5.4. Chemical Spray Pyrolysis (CSP)**

Chemical spray pyrolysis (CSP) is one of the solution based coating technique to produce metallic and semiconductor thin or thick films. Apart from the many other thin film fabrication methods, this technique is quite simple and comparatively cost-effective. Dense, porous or multi-layered films in any composition can be fabricated using this versatile method.

Temperature control unit, substrate heater, deposition solution and atomizer are components of the CSP setup. Schematic diagram of spray pyrolysis setup is given in Figure 1.9. Different type of atomizers such as air blast, ultrasonic or electrostatic can be employed depending on properties of liquid and operating conditions to obtain coatings with desired properties. Atomized droplets of deposition solution spread over the surface of the substrates with respect to the temperature of substrate, volume and momentum of the droplets. The interaction of droplets with substrate surface, aerosol transport, evaporation of solvent and decomposition of precursor are consecutive or simultaneous processes of this processing technique and these processes are accompanied by decomposition temperature [89]. Therefore, temperature is the main parameter of CSP and significantly affects the microstructural, optical and electrical properties of the resultant thin film. Moreover, air flow rate, nozzle distance and viscosity of deposition solution are the other controllable processing parameter to produce high quality coatings.

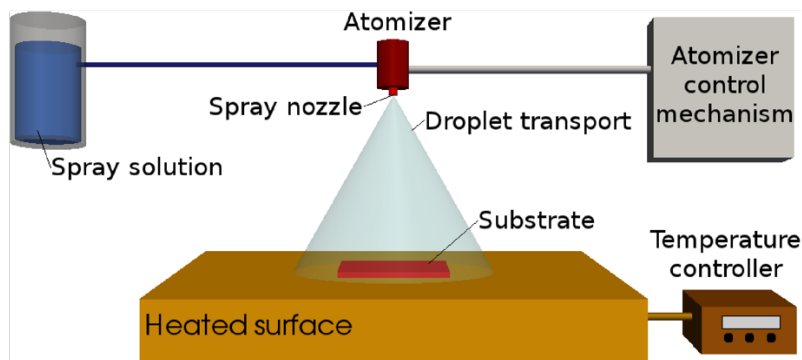


**Figure 1.9.** The general simplified scheme for spray pyrolysis, retrieved from [90].

### 1.5.5. Sol-gel Processing

Sol-gel processing is one of the main solution deposition techniques of thin films. ‘Sol’ includes metal alkoxides or metal salts as precursors (starting material) and their appropriate solvents. Moreover, sol may contain some functional additives such as stabilizers that chemically improves the homogeneity of sol. The liquid-filled solid network called ‘gel’ is originated by the linking colloidal particles with one another in 3D structure. The transformation from sol to gel is most commonly induced by changing the pH value of the sol via catalysts such as acids and bases. The catalysts initiate the sol to gel transformation by effecting the overall hydrolysis and condensation rates. As a result, characteristic of gel, such as structure of the chains or groups, time required for gelation. The effect of pH value on structure of gelation is given in Figure 1.10.

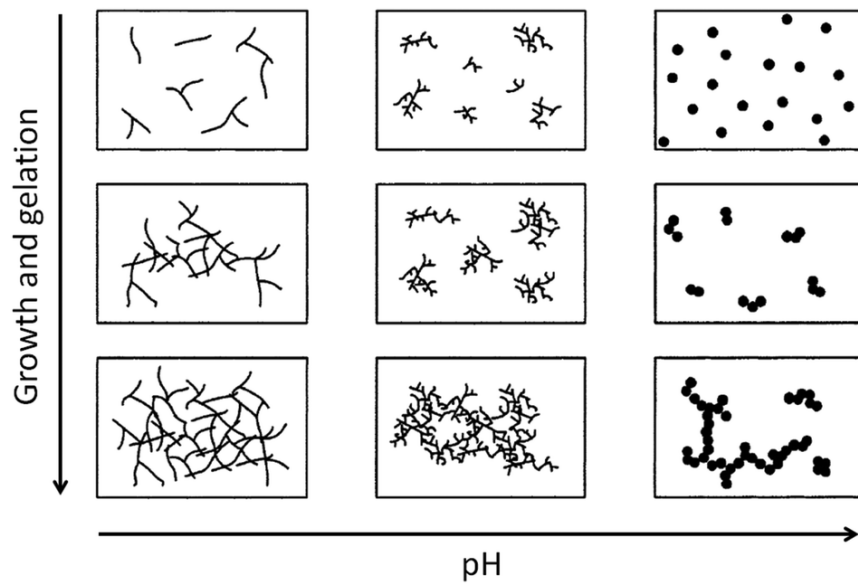


**Figure 1.10.** Effect of pH on structure of gel [91]

Sol-gel offers low temperature route for production of complex/functional oxide structures and deposition of sol onto complex-shaped or large surfaces [92]. It has several chemical and physical steps which are hydrolysis, condensation, drying and densification [93]. It is possible to fabricate high purity products such as micro and nano particles in different size/shape, fibers, membranes, powders and coatings by sol-gel process. The schematic summary of the sol-gel process is given in Figure 1.11.

There are three steps to form sol-gel based coatings as follows:

- i. Preparation of sol: sol particles forms by hydrolysis and condensation reactions at around room temperature.
- ii. Coating process: deposition of sol onto substrate by spray, dip or spin coating techniques.
- iii. Post deposition heat treatment: relatively high temperatures are applied to form crystalline and dense coatings.

This technique is promising with its low cost, simple equipment requirement and scalability. In addition, it allows stoichiometry-controlled production of multicomponent materials and the reproducible deposition of high purity thin films, practiced by spray, dip and spin coating techniques for the fabrication of thin film.

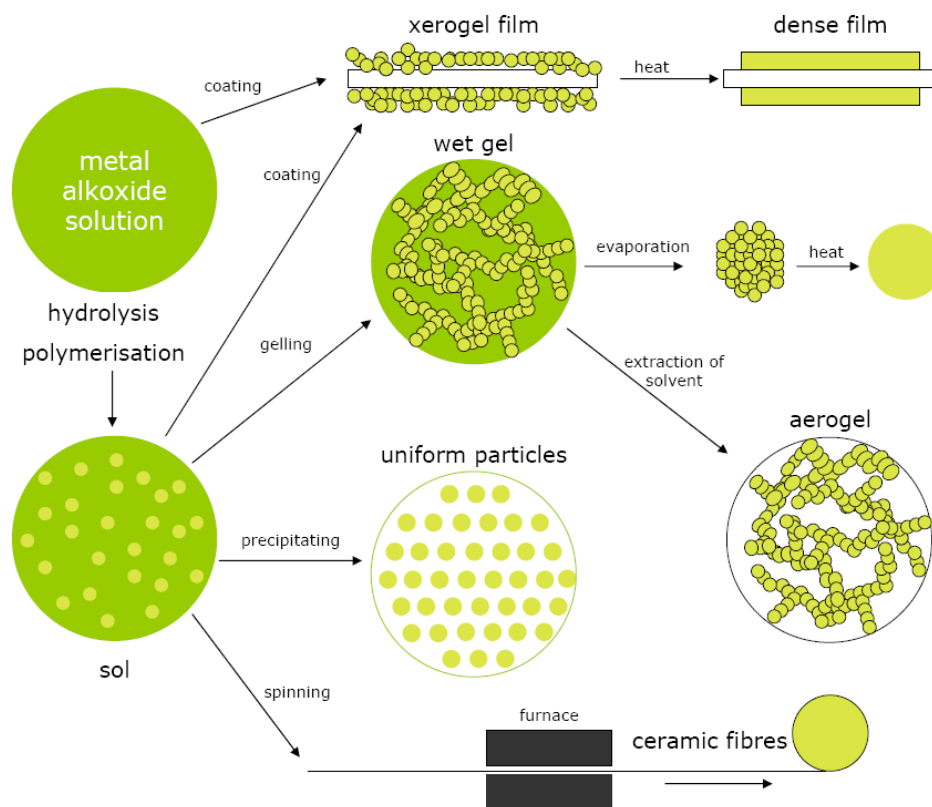


**Figure 1.11.** The schematic of sol-gel method, retrieved from [94].

## 1.6. Sol-gel Based Coating Techniques

### 1.6.1. Spray Coating

Dilute sol is sprayed onto the surface of the substrate. Scanning speed and spray pressure are controllable parameters for deposition. Boiling point of the sol and

wetting of substrate surface are important deposition parameters. Spray coating enables deposition onto complex surfaces, provides fast processing and requires low volume of sol; thus, it is efficient and widely used coating technique in industry.

### **1.6.2. Dip Coating**

Dip coating technique is the immersion of a substrate into the coating sol and subsequently withdrawing of substrate from sol or moving the sol away from the substrate for deposition of thin film. This technique allows the coating of both sides of the substrate simultaneously, large scale thin film production and offers the deposition of sol onto curved or complex-shaped substrates. Viscosity and density of sol and withdrawing speed of a substrate are determinants of the film thickness. The schematic illustration of the dip coating process is given in the Figure 1.12. Dip coating can be divided into four steps as follows:

- i. *Immersion*: the substrate is immersed into the coating sol at a constant rate.
- ii. *Hold time*: the dipped substrate is holding in the sol for a determinate period of time to allow the penetration of sol particles
- iii. *Deposition*: sol is deposited on the both sides of substrate while substrate is pulled up at a constant rate without any vibrations. Thickness of the film is dependent on this withdrawal speed such as, a thicker film is produced due to the higher speed.
- iv. *Evaporation*: draining of excess amount of sol and evaporation of a solvent from the deposited film. The evaporation process has already started throughout the deposition step, if solvent is volatile, such as alcohols.

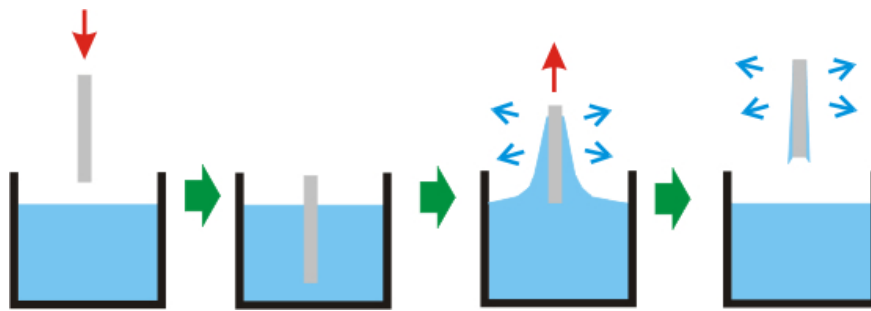


**Figure 1.12.** Schematic illustration of dip coating technique, retrieved from [95].

### 1.6.3. Spin Coating

Spin coating is widespread practice to obtain quite dense and uniform thin films from few nanometers to few micrometers in thickness on flat surfaces. Spin coating enables the production of single/multi-layered thin films quick, easy and reproducible; therefore, it is widely used in variety of industries and technological applications. However, the foremost weakness of this technique is that spin coating is applicable on flat surfaces only.

This technique is mainly based on the draining by centrifugal force and evaporation of solvent deposited thin film. Duration and speed of spin, viscosity and surface tension of sol, volatility of the solvent used in formation of sol are detrimental parameters to achieve dense, smooth and uniform coatings. Spin coating process is composed of four steps which are deposition, spin-up, spin-off and evaporation. These steps are given in Figure 1.13. schematically.

- i. *Deposition:* to get completely wet surface, surface of the substrate is coated by excess amount of sol.
- ii. *Spin-up:* substrate is accelerated up to the final selected speed for desired time; therefore, by the effect of centrifugal force, sol covers all over the surface and excess of the sol is flung off the surface.

- iii. *Spin-off*: substrate starts spinning at constant speed. In this step, viscous forces lead to fluid thinning mechanism and edge effects are commonly observed due to the high spin speed.
- iv. *Evaporation*: coating thinning mechanism dominates and almost all solvent evaporates simultaneously in this step of the processing; since, solvents used in composition of sol is typically volatile, such as alcohols. Transformation from sol to gel starts following evaporation of solvent.

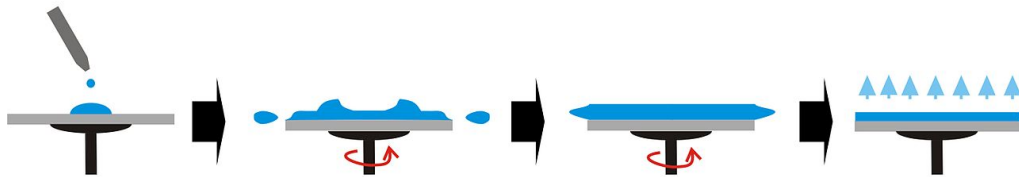


**Figure 1.13.** Schematic illustration of spin coating process, retrieved from [96].

## 1.7. Preparation of NiO Coating Sol: Processing Details

### 1.7.1. Nickel Precursors

Deposition sol of NiO is limited due to the lack of proper precursors having adequate solubility and stability in alcohol solvents. Nickel precursors employed in preparation of NiO coating sol can be broadly divided into two groups: nickel salts and organic compounds of nickel (alkoxides of nickel  $[(Ni(OR)_2)_n]$ ). Nickel sulphate heptahydrate ( $NiSO_4 \cdot 7H_2O$ ), nickel chloride ( $NiCl_2$ ) and nickel nitrate hexahydrate ( $Ni(NO_3)_2 \cdot 6H_2O$ ) are widely used nickel salts as starting materials to obtain NiO thin films. The high availability and the low cost of nickel salts compared to the organic compounds make them mostly preferred nickel precursors. Although nickel salts are

almost insoluble in organic solvent, they have reasonable solubility and stability in alcohol solvents, water or diols. However, metal salts are disposed to decompose irregularly resulting non-uniform particle size distribution and leave microstructural residuals at low annealing temperatures after deposition. Higher annealing temperatures can be applied to remove residuals; however, it can also cause the formation of cracked to a porous microstructure resulting in the change in desired optical and/or electrical properties of the film. Additionally, serious doubts about thermal instability of nickel nitrate are restricted the use of this precursor in large-scaled applications, although its high solubility in alcohol solvents [97].

Organic compounds of nickel are the other alternative Ni source for deposition of NiO thin films. Nickel acetate tetrahydrate ( $\text{Ni}(\text{CH}_3\text{COO})_2 \cdot 4(\text{H}_2\text{O})$ ) and nickel 2-ethylhexanoate ( $\text{C}_{16}\text{H}_{30}\text{NiO}_4$ ) are mostly preferred organic precursors to obtain coating sols. High cost and limited availability are the main drawbacks of metal-organic compounds. Moreover, high sensitivity of coating sols derived from organic precursors to environmental factors (e.g. temperature, humidity) limits their shelf life and restricts their employment in industrial applications. On the other hand, organometallic compounds have high solubility and stability in organic solvents through their organic ligands and some of them also offer solubility in water and alcohol solvents. Furthermore, lower temperatures compared to the metal salts are sufficient to remove organic residuals from the microstructure.

In general, there are limited number of nickel compounds (both salts and organics) used as precursor in NiO deposition sol. The number of suitable solvents providing complete dissolution of Ni precursors are insufficient; therefore, synthesis of different nickel complexes has been reported in literature [97]. Studies are especially focused on the synthesis nickel precursors derived from nickel alkoxides because of their high purities. Donor functionalized groups, such as dimethylaminoisopropoxide [ $\text{OCH}(\text{Me})\text{CH}_2\text{NMe}_2$ ] have been employed in order to achieve soluble nickel alkoxides complexes; however the product mixture could not be separated from its by-products.

Nickel  $\beta$ -diketonatalkoxides have also been synthesized as a nickel source material for sol-gel based coatings, but these compounds do not have solubility in alcohols. Then alcohol soluble Ni(II)-acetate and Ni(II)-acetylacetonone complexes and their derivatives such as,  $[\text{Ni}(\text{acac})_2]_3$  ( $\beta$ -diketonate derivate) and  $[\text{Ni}(\text{acac})_2(\text{py})]_2$  (derived by nitrogen ligands) etc., have been synthesized.  $[\text{Ni}(\text{acac})_2(\text{H}_2\text{O}_2)]$  and  $[\text{Ni}(\text{CH}_3\text{CO}_2)_2(\text{H}_2\text{O}_4)]$  are also known Ni(acac) complexes; however, they have poor solubility in alcohols at room temperature.

In literature, the most promising organic nickel compound derived from Ni(ac) has been synthesized by the complete breakdown of  $[\text{Ni}(\text{acac})_2]_3$  to mononuclear structure  $[\text{Ni}(\text{acac})_2(\text{dmaeH})]$  or  $\text{Ni}(\text{CH}_3\text{CO}_2)_2(\text{dmaeH})$  by addition of  $[\text{HOCH}_2\text{CH}_2\text{NMe}_2](\text{dmaeH})$  containing both donor functions of nitrogen and oxygen. Nickel complex of  $[\text{Ni}(\text{acac})_2(\text{dmaeH})]$  or  $\text{Ni}(\text{CH}_3\text{CO}_2)_2(\text{dmaeH})$  as a starting material have been used in deposition sol of NiO thin film for electrochromic applications by several authors [11, 98].

### 1.7.2. Solvents and Stabilizers

In solution-based processing, main function of solvents is providing proper medium for ingredients. Solvents are responsible to initiate and control the molecular level reactions. The significant parameters of solvents such as density, boiling point, molecular weight and polarity are the determinants of the nature of sol and following thin film formation processes. Drying and annealing practices also depend on the solvent characteristics. In literature, suitable solvents of Ni salts are given as alcohols (ethanol, isopropanol, butanol etc.) [99], isopropanol/butanol-ethylene glycol mixtures [1], ethylene glycol [100]. Alcohols (isopropanol and ethanol) [12, 101], 2-methoxyethanol [10], 3-methoxyphenol [102] and dimethylaminoethanol [11] are used for dissolution of organic compounds of nickel.

Chelating agents and stabilizers are commonly used to organize the rate of subsequent reactions, such as hydrolysis and condensation, during the formation of deposition sol.

Bonding between the separate binding sites with the equal ligands (chelating or sequestering agents) around the single same central atom is called chelation. Supporting the chemical homogeneity of sol is the significant function of chelating agents via coordinating metal cations or ions through usually oxygen atoms. Thereby, metal cations/ions are homogeneously distributed in molecular level resulting the thin film formation with chemical structure in order. Regular structure leads to improve the desired properties of the resultant film. The other main role of chelating agent is reducing the rate of hydrolysis and condensation reactions. Especially for organic precursors, suppressing the rate of condensation and controlling subsequent reactions are essential to prevent the precipitation problems. The binding strength of ligands of chelating agent / precursor ratio has effects on the structural consequences for the final gel. If the number of –OR decreases, the sites are reduced for hydrolysis and less crosslinking are induced in the resultant gel. This control mechanism of metal cations/ions via chelating agents facilitates obtaining of different products from amorphous to crystalline in sol-gel processing [91, 103].

Mostly used chelating agents for NiO sols are 3-aminopropyl triethoxysilane [99] (APTES), N-[3-(trimethoxysilyl)propyl]-ethylendiamine (DAEPTMS) [99], amorphous polyethylene oxide (a-PEO) [100], sodium hydroxide [9], monoethanolamine (MEA) [10], acetic acid [8], glycerol [104], polyvinyl alcohol (PVA) [105], ammonium hydroxide [1] and dimethylaminoethanol (dmaeH) [97]. It was reported that the MEA and dmaeH are also used as stabilizer [10].

### **1.8. Parameters Affecting the Quality of Sol-gel Deposited NiO films**

There are some restrictions/problems in the deposition of NiO thin films by sol-gel processing. In this section, limitations are described and some of the solutions reported in literature are discussed.

### 1.8.1. Annealing Temperature

Post deposition heat treatment (namely, calcination or annealing temperature) is one of the significant controllable parameter to fabricate thin films with desired microstructural, optical and electrical properties. Sol-gel deposited NiO thin films generally requires heat treatment in order to induce crystallization and remove inorganic/organic residuals. Annealing temperature is determined by the sol characteristics, i.e. nature of Ni precursor, solvent or chelating agent. More crystalline and conductive films are obtained with an increase in annealing temperature whereas the optical transparency of the films decreases. Annealing temperature can be roughly determined by the thermal decomposition temperature of precursor and temperature required to remove organic/inorganic residuals.

NiO thin film annealed at 400 °C is composed of particle clusters with pores; therefore loose packaging is observed [100]. As temperature increases (450 °C and above), particles become well-packaged and highly crystalline resulting in the reduction of the density of pores and the grain boundaries. As a result of that, optical transparency of the NiO film in visible region change slightly and the shift in optical absorption spectrum is observed. Hence, the optical band gap ( $E_g$ ) of the films decrease with increase in annealing temperature [102].

NiO thin films annealed at higher temperatures have higher electrical conductivity [106] that can be explained by an increase in both particle size and intimate particle contact. Charge carriers can easily find new pathways for conduction; therefore, decrease in the activation energy is observed.

On the other hand, higher annealing temperatures can radically induce microstructural crack formation and increase surface roughness [100]. Additionally, strain point of glass substrate (572 °C) and diffusion of alkali ions ( $Ca^+$ ,  $Na^+$  etc.) from underlying glass to coating restricts to annealing temperatures above 550 °C [107]. Glass substrates (i.e. borosilicate or quartz) that do not include alkali ions are utilized in order

to overcome these limitations. Moreover, optical transparency is the other key parameter for substrates. Optical transmission region of the substrate should be correlated that of optical properties of thin film. For example, alkali free glass substrate is quite transparent to the visible part of spectrum; whereas, it has no optical transparency in UV region (300 nm and below). Thereby, quartz substrate may be utilized for investigations in UV region of the optical spectrum due to its high UV transparency.

### **1.8.2. Thin Film Thickness**

Thin film thickness is controllable parameter in sol-gel processing which makes the thin film properties tunable. NiO thin films with various thicknesses between several nanometers to sub micrometers can be deposited by sol-gel processing. Increase in sol molarity and the number of coating operation (coating-drying cycle) increase thin film thickness.

Thin film thickness increases almost linearly with the number of coating layers and molarity of coating sol [108, 109]. Relation between thin film thickness and coating layers is given in Figure 1.14. Thin film thickness can also be changed by the molarity of deposition sol. Especially in very thick thin films, dense and uniform films with precise thicknesses can be achieved by repeating the coating-drying cycle. Even repeating the coating process subsequently is not useful for industrial applications, this technique offers the precise control of thin film thickness and dense/uniform film formation.

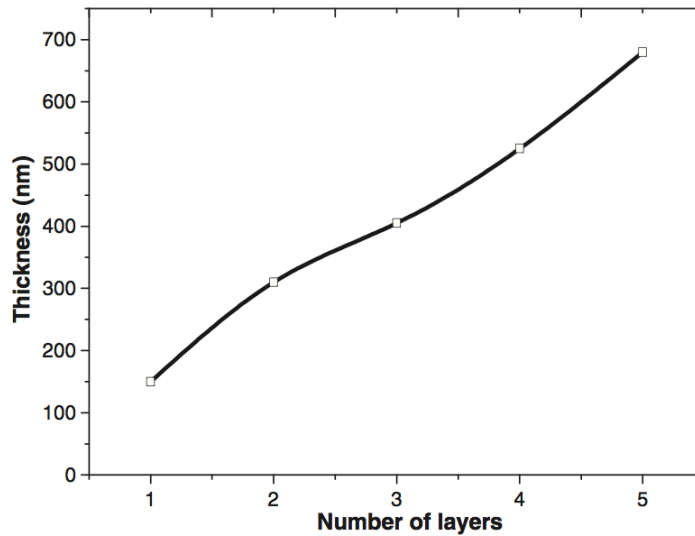


**Figure 1.14.** Effect of number of layers on thickness of NiO thin films [110].

Increase in the number of operated layers enhances the grain size of NiO thin films. Variation of the grain size with the number of coating layers is given in Figure 1.15. Due to the increase in grain size, surface roughness of the films also increases. Mobility of the molecules on the surface is enhanced, so increase in grain size is observed when the number of coating layers increases [108, 110].

On the other hand, increase in grain size promotes the electrical conductivity of the films. Resistivity of the film decreases with increase in thickness and grain size. Enhancement in electrical conductivity with increasing grain size can be explained by reduction in grain boundary scattering of charge carriers.

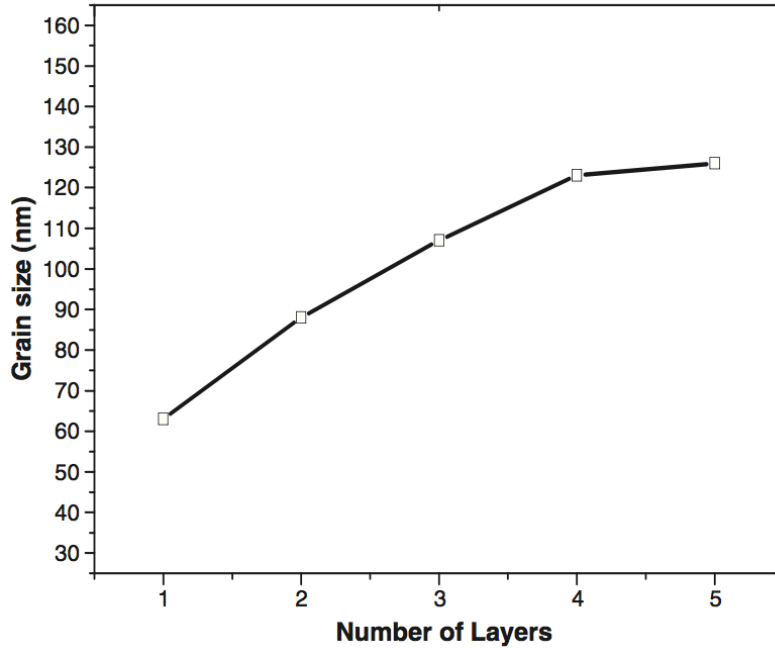


**Figure 1.15.** Variation of the grain size with the number of layers constituting NiO films [110].

Additionally, optical band gap of the films is also changed by the effect of film thickness. Band gap of bulk crystalline NiO is nearly 4.0 eV [31, 111]; however, in thin film form, gap decreases up to approximately 3.65 eV [110]. The reason of this change in band gap is considered as amorphous structure. Electronic transition mechanism of amorphous states whether through localized states in conduction band or extended states in the valence band to localized states at the conduction edge. This leads to lower energies than those for polycrystalline or bulk crystalline materials. Effect of film thickness on optical band gap of the films is given in Figure 1.16.

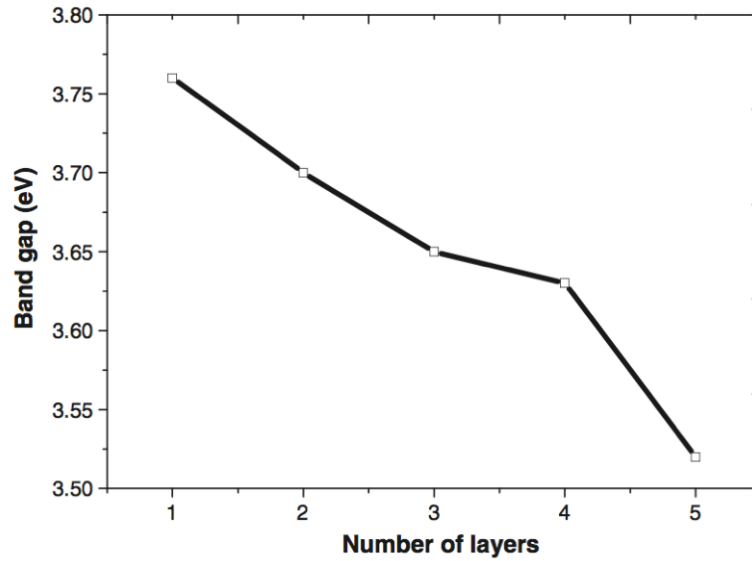


**Figure 1.16.** Effect of number of layers on the optical band gap of NiO films [110].

### 1.9. Objective of the Thesis

The aim of this study is to challenge and overcome some of the previously stated problems (Section 1.8. Parameters effected the quality of the sol-gel deposited NiO thin films) related with formation of NiO thin films by sol-gel technique. The specific objectives of this thesis can be summarized as follows:

- Deposition of NiO thin films on glass substrates by sol-gel spin coating method using an organic nickel precursor,
- Controlling the thin film thickness and NiO particle size in reproducible manner by the use of deposition parameters (duration and speed of spinning) and the post deposition heat treatment parameters (drying and annealing temperature and conditions) to develop crack free and homogeneous coatings,

- Investigation of the effect of the number of processing parameters (coating, heat treatment) on microstructural, optical and electrical properties of the resultant films.

## CHAPTER 2

### MATERIALS AND METHODS

In this chapter the materials used in the fabrication of spin-coated NiO thin films are listed and the experimental procedures are explained. Additionally, analytical techniques that have been used to investigate the film properties are described.

#### 2.1. Materials

The list of the chemicals used in this study are given in Table 2.1. All chemicals were used as supplied without any purification.

**Table 2.1.** List of chemicals used in NiO sol preparation.

Material	Supplier	Purity	Formula
Nickel (II) acetate tetrahydrate	Sigma Aldrich	98%	$\text{Ni}(\text{CH}_3\text{COO})_2 \cdot 4(\text{H}_2\text{O})$
2-methoxyethanol	Fluka	99.5%	$\text{C}_3\text{H}_8\text{O}_2$
Monoethanolamine (MEA)	Sigma Aldrich	98%	$\text{C}_2\text{H}_7\text{NO}$

#### 2.2. Experimental Procedure

##### 2.2.1. Cleaning Procedure of Glass Substrates

Soda-lime-silica glass substrates (or SLS, precleaned microscope slides, Gold Seal

25x25 mm) were cleaned consecutively by acetone, isopropanol and deionized water for 20 min using an ultrasonic bath. At the end, substrates were dried under nitrogen flow.

### 2.2.2. Preparation of Coating Sol

Coating solution is composed of nickel (II) acetate tetrahydrate as the precursor, 2-methoxyethanol as the solvent and monoethanolamine (MEA) as the stabilizer. 2mM of nickel (II) acetate tetrahydrate was dissolved in 20 mL of 2-methoxyethanol at room temperature, 0.12 mL of MEA was added to the mixture. The solution was mixed by stirring at 60 °C for 2 h in a closed container. After cooling down to room temperature, solution was used for the coating process. A flowchart for preparation of the coating sol is provided in Figure 2.1.

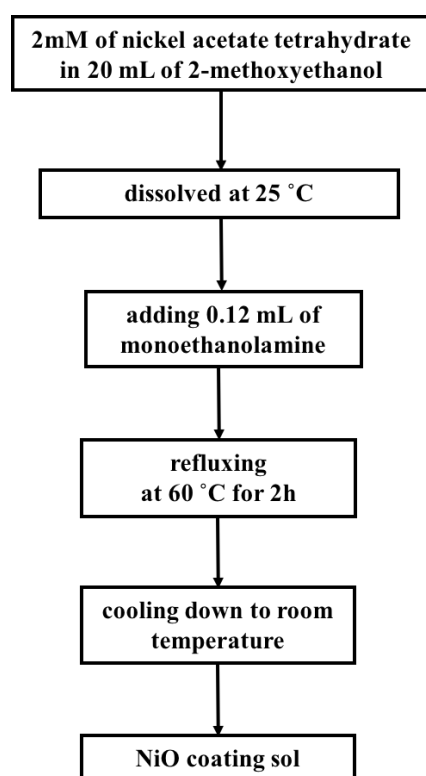


**Figure 2.1.** Processing details for preparation of NiO coating sol.

### 2.2.3. Deposition of NiO Thin Films

Deposition of coating sol onto glass substrates by using spin coating technique with Specialty Coating System<sup>TM</sup> G3 spin coater. Spin coating was applied at 3000 rpm for 30 s. At the end of coating step, films were dried at 180 °C for 15 min in an oven to remove the organics. In order to obtain homogeneous and dense layers, spin coating process and drying step was repeated for 5, 10 and 15 times. Following deposition, films were gradually annealed at 400, 450 or 500 °C for 30 min under ambient conditions. The heating rate was 5 °C/min. Formation of NiO film from nickel acetate sol involves condensation and thermal mixing with decomposition. These occur by evaporation of the solvent and surface agent during drying and also during the high temperature annealing steps. It was reported that dehydration and decomposition of nickel acetate tetrahydrate reaches to completion around 350 °C and conversion to NiO is expected to occur temperatures higher than 350°C accompanied with the decomposition of residual solvent and stabilizer [13]. Therefore, minimum annealing temperature was determined as 400 °C. On the other hand, 500 °C was chosen as maximum annealing temperature; since, soda-lime-silica glass softens at is around 570 °C [1]. The flowchart of the production of NiO thin films is given in Figure 2.2.

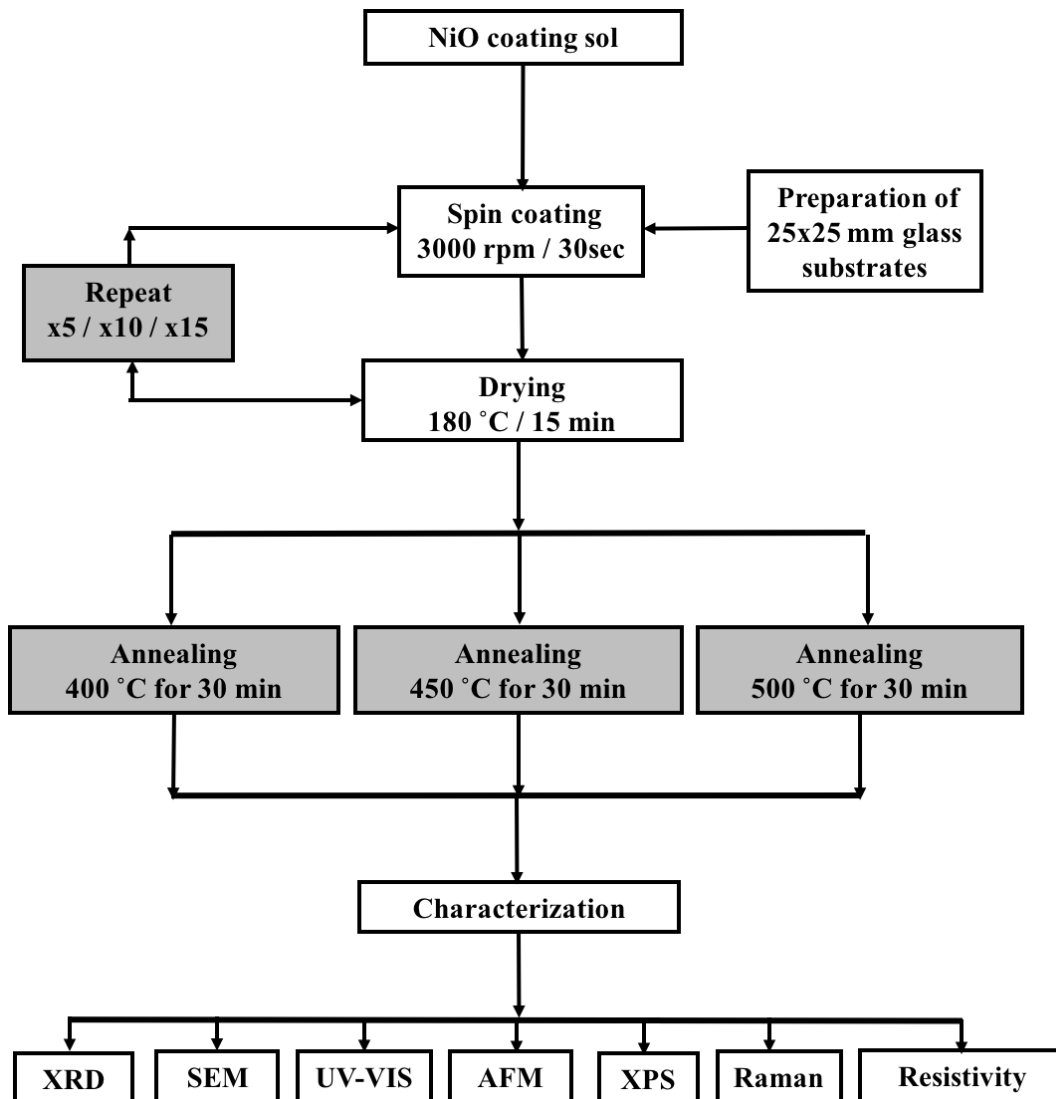


**Figure 2.2.** Experimental procedure for fabrication of NiO thin films

### 2.3. Materials Characterization

In this section of the thesis, analytical characterization techniques used in investigation of microstructural, morphological and optoelectronic properties of sol-gel deposited NiO thin films are presented in detail. X-ray diffraction (XRD) method was used to determine the crystal structure and assess the crystallinity of NiO thin films. The surface morphology of the films was investigated by atomic force microscopy (AFM) and scanning electron microscopy (SEM). Structural analyses were examined by

Raman spectroscopy. Electronic characteristics and surface chemical analyses of the films were performed by X-ray photoelectron spectroscopy (XPS). UV-Vis spectrophotometry was used for determination of the optical transparency and the optical band gap of the films. Finally, temperature-dependent resistivity measurements of the films were carried out using two-probe method for investigation of electrical properties of the films.

### **2.3.1. X-ray Diffraction (XRD)**

X-ray diffraction (XRD) analyses were performed to examine the transition from amorphous to crystalline state and determine the crystal structure of nanostructured NiO films after heat treatments. A Rigaku Miniflex system equipped with Cu K $\alpha$  radiation (0.154 nm) was used. The diffraction tests were performed for diffraction angle ( $2\theta$ ) between 20° and 80° at a scan rate of 1°/min.

### **2.3.2. Atomic Force Microscopy (AFM)**

Atomic force microscopy (AFM) was used to investigate the surface morphology of the films with a Veeco MultiMode V model in tapping mode. Microstructural details and roughness of the film surface were examined at sampling sizes of 1 x 1  $\mu\text{m}$  and 200 x 200 nm.

### **2.3.3. Scanning Electron Microscopy (SEM)**

Scanning electron microscopy (SEM) analyses were conducted for microstructure and thickness examinations using a FEI Quanta 400 FEG equipped with energy dispersive X-ray analyzer operated at 20 kV. A gold layer of approximately 2-3 nm was deposited onto samples in order to reduce the charging effects during SEM analyses.

### **2.3.4. X-ray Photoelectron Spectroscopy (XPS)**

Surface chemical nature of the films were investigated by X-ray photoelectron spectroscopy (XPS). XPS analyses were conducted using a monochromatic Al K $\alpha$  X-

ray source (1486.6 eV) with a PHI 5000 VersaProbe. Nominal binding energy of the C 1s was 284.5 eV. The XPS spectra of Ni 2p and O 1s core levels were recorded.

### **2.3.5. Raman Spectroscopy**

Raman spectroscopy was used for investigation of vibrational, rotational and low-frequency modes in the crystal in order to confirm the thin film formation and determine the crystal structure. Raman spectra of the films were recorded using monochromatic 532 nm Nd-YAG laser.

### **2.3.6. UV-Vis Spectrophotometry**

UV-Vis light transmission of the films were recorded within the wavelength range of 200 to 800 nm using Cary100 Bio-Varian UV-Vis Spectrophotometer and air measurements were taken as a background. According to the optical transmission spectra of the films, optical band gaps of the films were estimated.

### **2.3.7. Temperature-dependent Resistivity Measurements**

Temperature-dependent resistivity measurements were performed by two probe method using Yokogawa GS610 source measure unit to examine the electrical conduction mechanism of the films. The measurements were carried out under a bias of 5 V at ambient conditions. 100 nm thick evaporated gold contacts that were 500  $\mu\text{m}$  apart were used for the measurements.

## CHAPTER 3

### RESULTS AND DISCUSSION

NiO thin films were formed on glass substrates by spin coating of sol-gel derived solutions. The film formation behavior, structural, morphological and optoelectronic properties of the films were investigated as a function of controllable processing parameters, such as thin film thickness and post deposition heat treatment (annealing temperature) in the range of 400-500 °C. This chapter starts with the structural and morphological properties of NiO thin films and continues on investigation of optoelectronic properties.

#### 3.1. Structural and Morphological Properties of NiO Thin Films

##### 3.1.1 XRD analyses

XRD patterns of the NiO thin films annealed at 400, 450 and 500 °C were obtained to determine the crystal structure and assess the crystallinity of the films. XRD analyses confirmed the formation of crystalline NiO thin films after annealing. XRD diffractograms of NiO thin films are provided in Figure 3.1. The films are composed of pure NiO cubic and peaks at 37 ° (111), 43 ° (200) and 63 ° (220) are assigned to bunsenite phase according to JCPDS file 711179. No other secondary phases within the detection limit of XRD such as nickel hydroxide [Ni(OH)<sub>2</sub>] or nickel (III) oxide [Ni<sub>2</sub>O<sub>3</sub>] were observed. This is particularly important because these phases were reported as by-products of sol-gel deposited NiO films [112, 113]. The diffraction peaks are not quite distinctive for films annealed at 400 °C and the pattern is dominated

with an amorphous hump. The intensity of the peaks increases with annealing temperature indicating the crystallinity of the films strongly improves with the annealing temperature. Films annealed at above 400 °C clearly exhibit crystallinity as evidenced by relatively better well-defined peak shapes. Diffraction peaks are sharper for the sample annealed at 450 °C and 500 °C and full width at half maximum values decrease with increasing temperature suggesting that crystallite size increases with temperature.

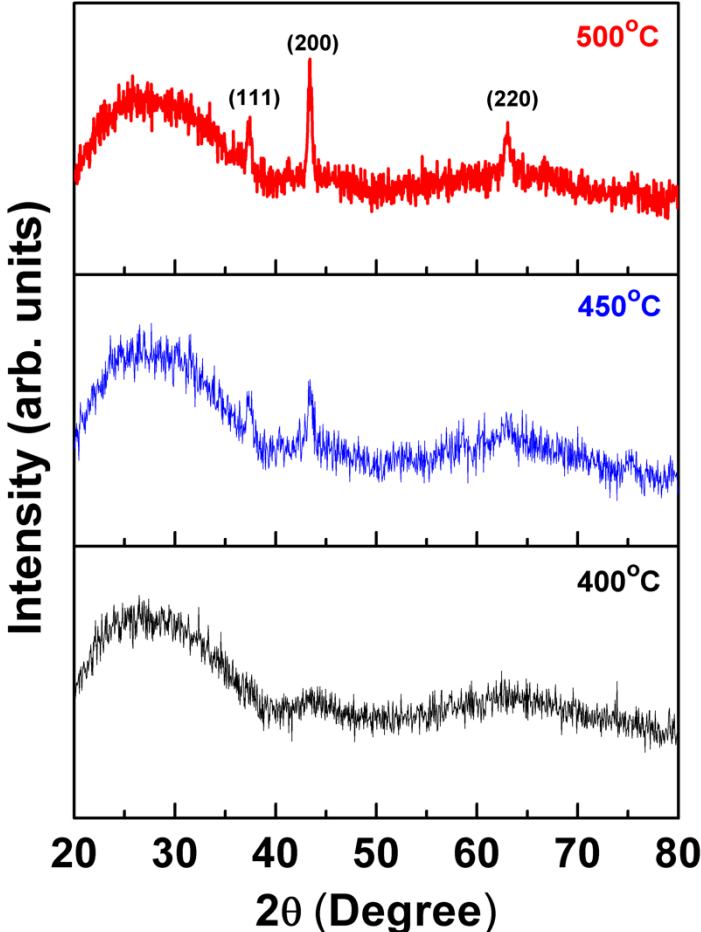


**Figure 3.1.** XRD diffractograms of 15 times coated NiO films annealed in air at different temperatures.

### 3.1.2. AFM analyses

The crystallite size variation with annealing temperature as revealed by the XRD data has also confirmed by microstructural findings using AFM. 3D topographical images of 10 times coated films are shown in Figure 3.2. (a)-(f).

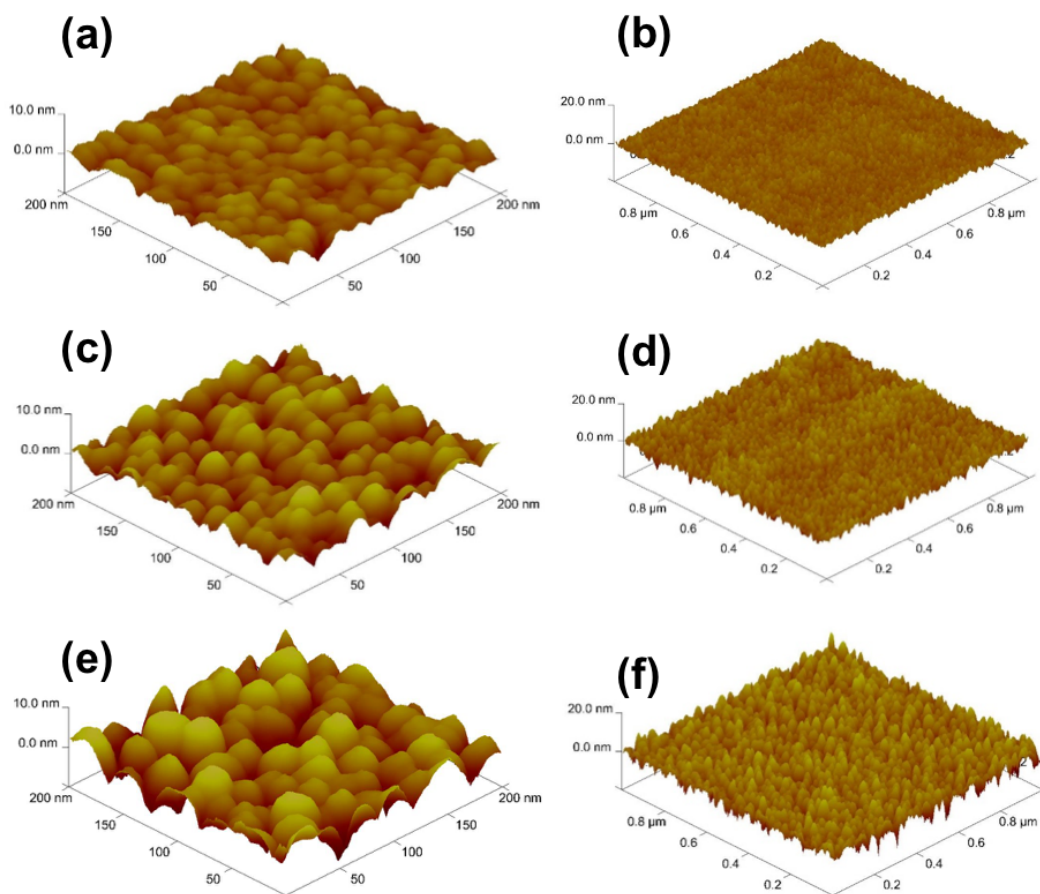


**Figure 3.2.** AFM images of 10 times coated NiO films annealed at 400 (a,b), 450 (c,d) and 500 °C (e,f)

The particle size of the films are measured as  $13 \pm 1$  nm,  $16 \pm 1$  nm and  $22 \pm 1$  nm for the samples annealed at 400, 450 and 500 °C, respectively. In addition to an increase in particle size, root mean square (RMS) roughness values of the films are found to

increase with the annealing temperature. RMS values were measured as 0.95, 2.70 and 2.70 nm for 400, 450 and 500 °C annealed samples, respectively. Increase in the particle size and roughness of the films can be explained with enhanced crystal growth and ripening of the individual small crystals due to thermal effect. Low roughness values clearly indicate that these films are extremely smooth and pristine. Film morphology is crack free without porosity with well-connected spherical nanofeatures. The absence of porosity and low roughness characteristics are critical for almost all optoelectronic device applications as cracks and pores, lead to shunt and recombination pathways and suppress the charge mobility and electronic conductivity, which are detrimental for device operation.

### **3.1.2 SEM analyses**

Apart from the AFM analysis, the morphological properties of the films were further characterized by SEM. SEM images of 5, 10 and 15 times spin coated films with corresponding thickness of 60, 110 and 170 nm are provided in Figures 3.3., 3.4. and 3.5. respectively. Each figure contains three top-view SEM images for films annealed at different temperatures and a cross-sectional detail images used in thickness determination. Film thickness correlates with the number of spin coating steps, and typically 10-12 nm thick layer can be deposited at each coating step. Films contain well-connected spherical nanoparticles, which eventually forms a dense and amorphous deposit over the glass substrates. Additionally, it was found that the annealing temperature does not directly affect the film thickness; therefore, only cross-sectional SEM images corresponding to different number of layers prepared at the same annealing temperature were represented in the figures.

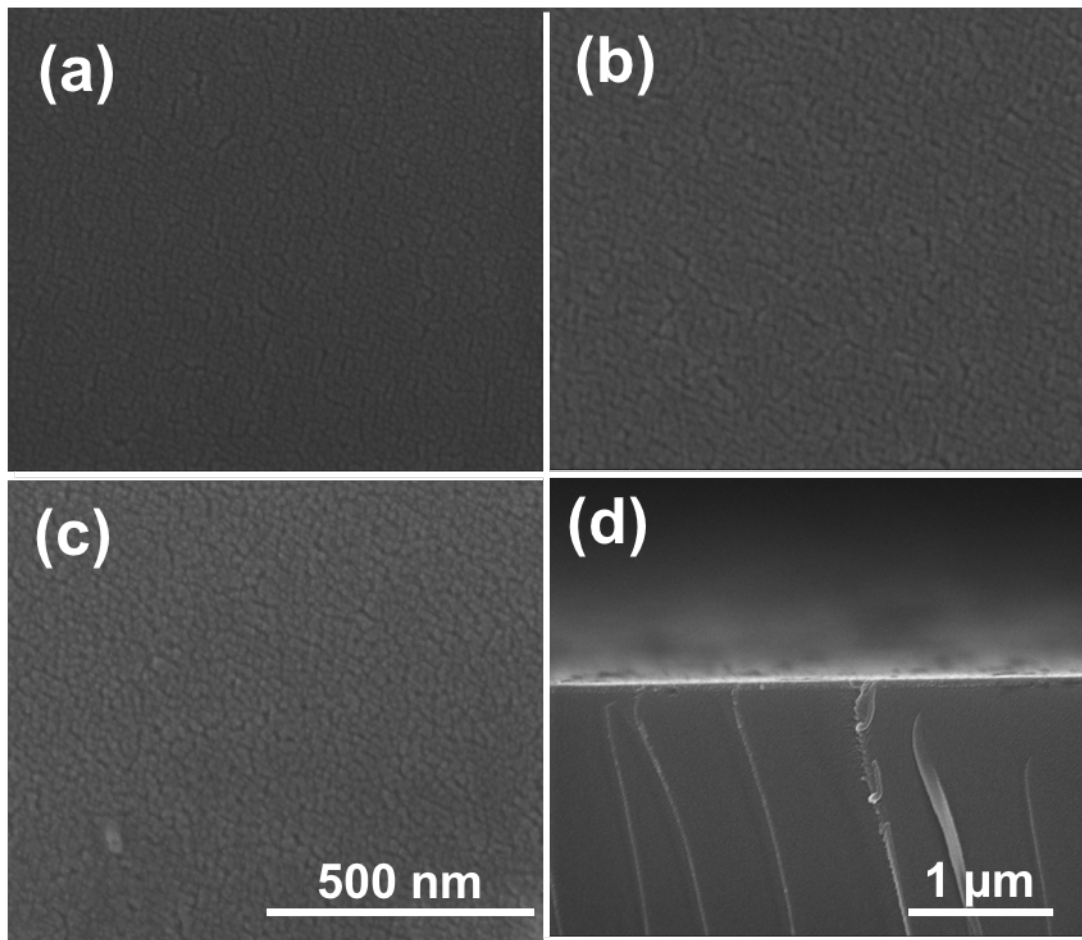


**Figure 3.3.** Top view SEM micrographs 60 nm thick NiO films annealed in air at **(a)** 400, **(b)** 450 and **(c)** 500 °C at the same magnification. **(d)** Cross-sectional SEM image of 60 nm thick NiO film annealed at 400 °C.

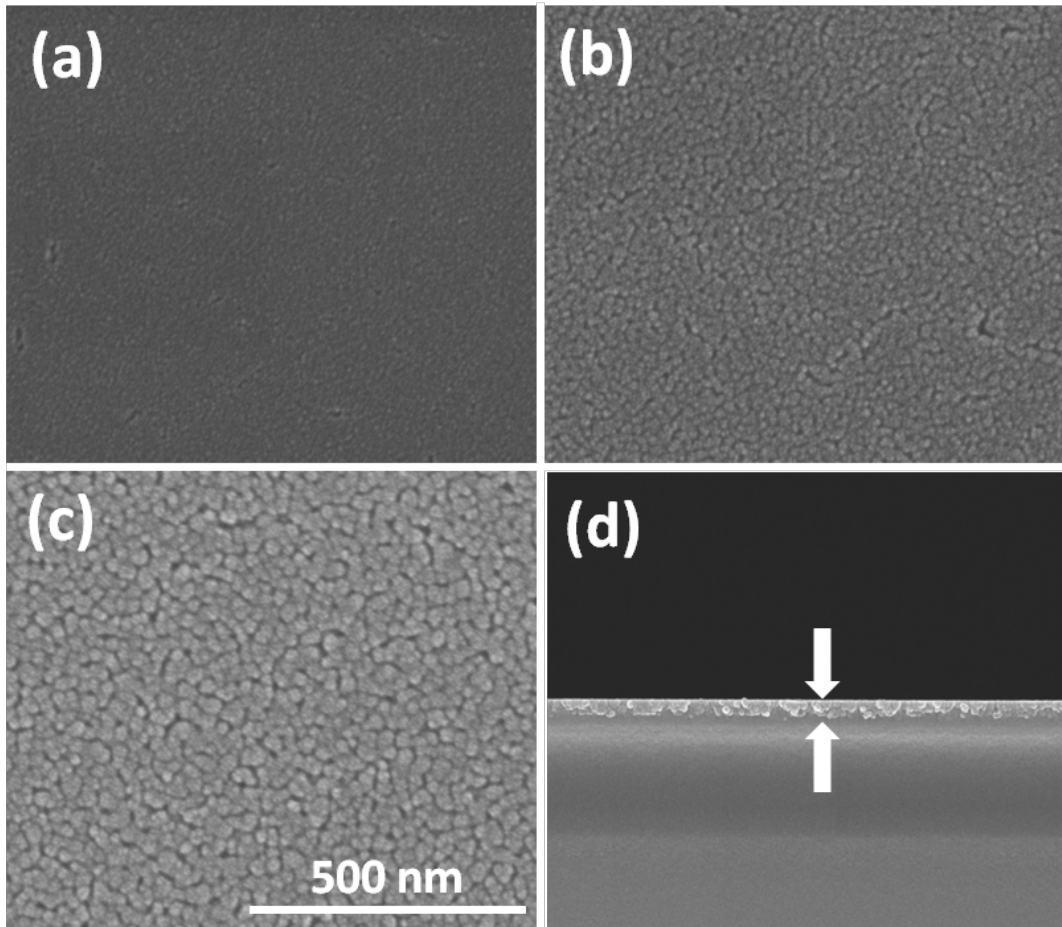


**Figure 3.4.** Top view SEM micrographs 110 nm thick NiO films annealed in air at (a) 400, (b) 450 and (c) 500 °C at the same magnification. (d) Cross-sectional SEM image of 60 nm thick NiO film annealed at 450 °C.

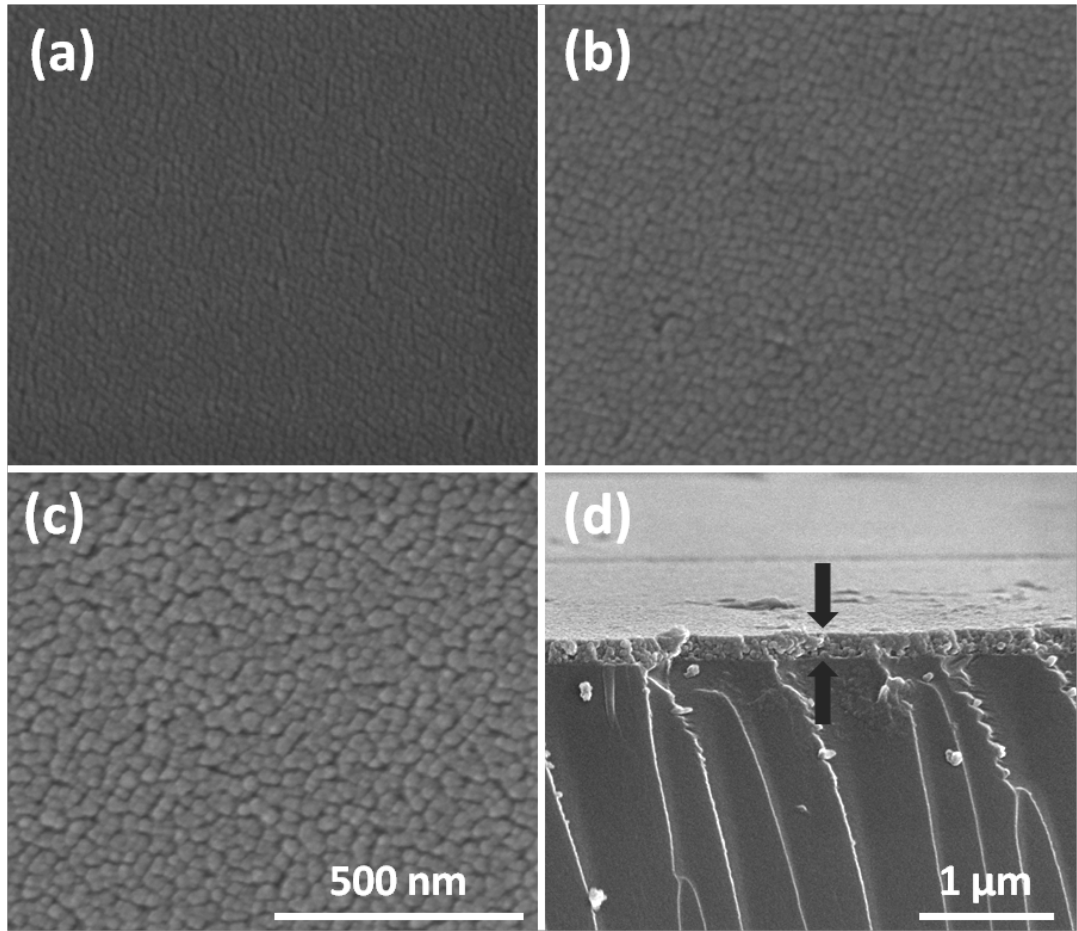


**Figure 3.5.** Top view SEM micrographs 170 nm thick NiO films annealed in air at **(a)** 400, **(b)** 450 and **(c)** 500 °C at the same magnification. **(d)** Cross-sectional SEM image of 170 nm thick NiO film annealed at 500 °C.

From the top-view SEM images, it was observed that the films are crack free and homogeneous, with extra fine particles distributed uniformly on the glass substrate for all film thicknesses and annealing temperatures. The average particle size for each film thickness and annealing temperature were measured and provided in Table 3.1. Together with the AFM results, it can be said that the particle size of the films clearly increases with increasing annealing temperature. The particle size also increases with

the film thickness. Thickness-dependent increase in the particle size can be explained by the enhancement of nanostructured film growth due to the number of drying steps between each spin coating steps, which leads to improved crystal growth.

**Table 3.1.** Average particle size and thickness of NiO films determined from the SEM micrographs using the instrument (FEI Quanta 400 FEG/C) image processing software (xTm Microscope Control).

Annealing temperature	60 nm thick film	110 nm thick film	170 nm thick film
400°C	9.7 ± 1 nm	11.9 ± 1 nm	14.4 ± 1 nm
450 °C	11.2 ± 1 nm	15.8 ± 1 nm	22.5 ± 1 nm
500 °C	14.9 ± 1 nm	21.9 ± 1 nm	29.2± 1 nm

### 3.1.3 Raman Spectroscopy

Structural analyses of the thin films have also been conducted through Raman spectroscopy. The respective Raman spectra are shown in Figure 3.6. In order to minimize the substrate originated reflections the thickest film with a thickness of 170 nm has been used in Raman measurements. Five vibrational bands were observed. Bands seen at 560, 740, 925 and 1100  $\text{cm}^{-1}$  due to 1 phonon (1P) longitudinal optical (LO) mode, 2P 2 transverse optical (TO) modes, 2P TO+LO and 2P 2LO scattering, respectively. Band at 1500  $\text{cm}^{-1}$  is assigned to 2 magnon (2M) excitation of pure NiO [114]. Because of the defect and surface effects of nanosized NiO, 1P band is very distinctive; whereas, 2P bands appear to be more broadened. 2M excitations are due to short-range magnetic interactions at the Brillouin zone boundary and the presence of 2M band in Raman spectra is evident of the remaining antiferromagnetic phase of nanocrystalline NiO at room temperature and  $\text{Ni}^{2+} - \text{O}^{2-} - \text{Ni}^{2+}$  superexchange

interaction [115]. It was observed that the intensity of 2M band decreases with a decrease in the particle size. Similarly, Mironova-Ulmane et al. reported that the intensity of 2M band of nanopowders produced from the evaporation of the coarse grained NiO nanopowders decreases with the decreases with a decrease in particle size [114].

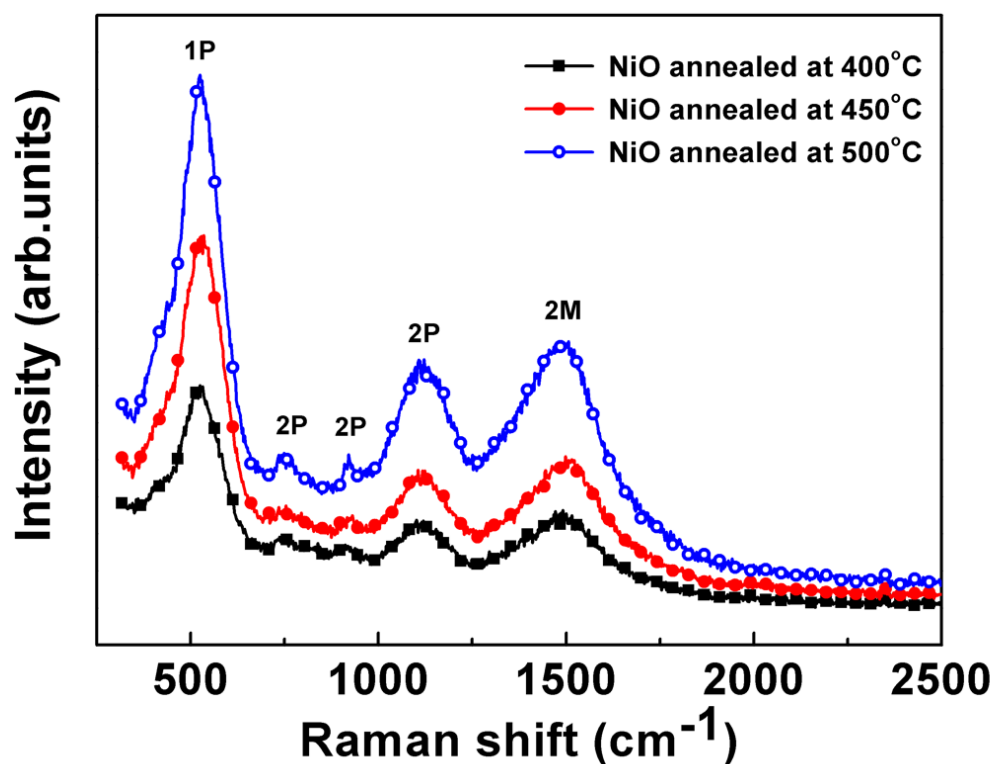


**Figure 3.6.** Raman spectra of 170 nm thick NiO films annealed at different temperatures.

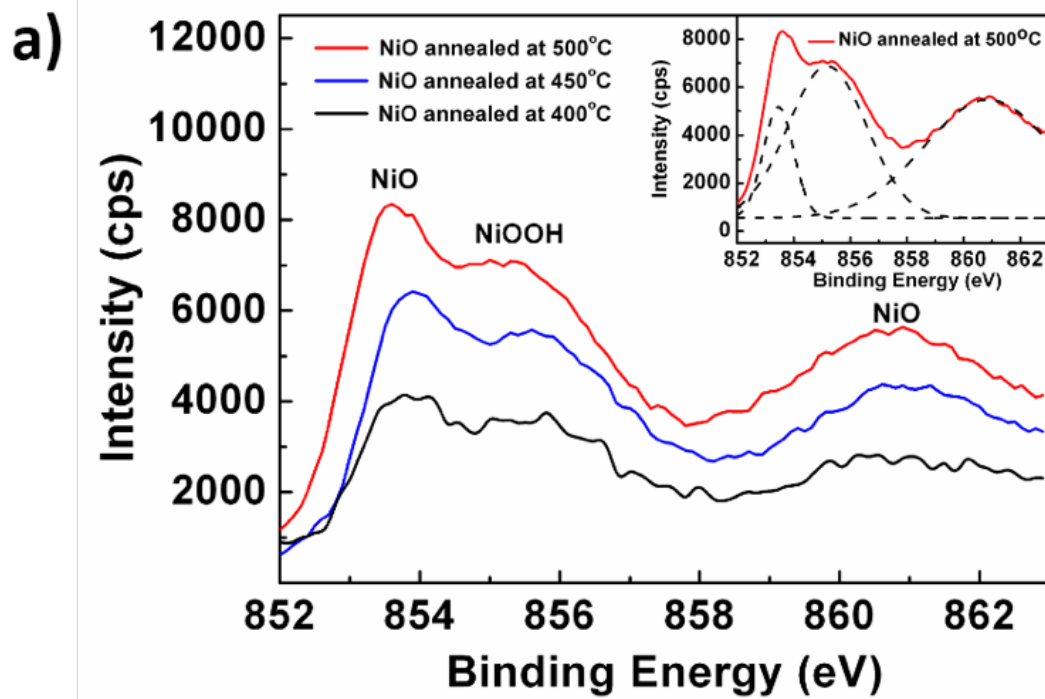
In addition, 2M band is undetectable for 100 nm particles at room temperature due to the decrease of antiferromagnetic correlations [114]. However, they observed 2M band from 13 nm NiO nanoparticles prepared by precipitation method [116]. Moreover, decrease in the intensity of 2M band of pure polycrystalline NiO prepared by thermal

decomposition was observed upon dilution with Mg ions due to the lowering of local symmetry at the Ni<sup>2+</sup> sites [117]. As a result of these observations, not only disorders due to the defects, but also the small particle size decreasing the spin correlation length lead to the lowering of 2M band [118]. The band at 560 cm<sup>-1</sup> arises from the strong phonon-magnon interaction at the surface or defects competing with the magnetic ordering of nanoparticles. It was reported that the band at 560 cm<sup>-1</sup> is affected by the annealing temperature, heating of the film due to the heat of laser and the particle size [116]. Similarly 2M band, intensity of band at 560 cm<sup>-1</sup> decreases with decreasing crystallite size [119]. These results indicate that the crystal quality of the films get improved with heat treatment and they are in agreement with the XRD results obtained for 170 nm thick films annealed at different temperatures.

#### 3.1.4 XPS Analyses

XPS spectra of the Ni 2p and O 1s core levels are given in Figure 3.7. (a) and (b), respectively. In figure 3.7. (a), the signal at 853 eV is assigned to Ni<sup>2+</sup> coming from 2p<sup>3/2</sup> levels with the satellite peak around 860 eV belonging to NiO phase [14]. The signal at 855 eV indicates the presence of Ni<sup>3+</sup>, which is commonly attributed to Ni<sub>2</sub>O<sub>3</sub> or NiOOH compounds. Also oxygen deficiency may lead to lattice distortion and causes charge imbalance, which in turn favors the formation of Ni<sup>3+</sup>. Since there is no evidence of the presence of other nickel-based phases in XRD and Raman, it is highly probable that the NiOOH forms on most outer top surface of the NiO films considering the surface sensitivity of XPS measurements. The presence of NiOOH could be attributed to the water adsorption and consecutive hydroxylation near the surface of the sample [120]. This can be further clarified by the features of O 1s signal. Related O 1s spectrum shows a Ni-O binding energy at 529.2 eV corresponding to the octahedral structure of NiO and a secondary signal at 531.2 eV, which is also attributed to nickel hydroxides and oxyhydroxides that forms in negligible amounts on the surface of the films. Although XRD results imply that the films annealed at 400 °C are poorly crystalline, if not totally amorphous, formation of NiO is evident from Raman

and XPS results. As evidenced by XRD, Raman and XPS results, coating sol has been fully converted to crystalline NiO film upon annealing.



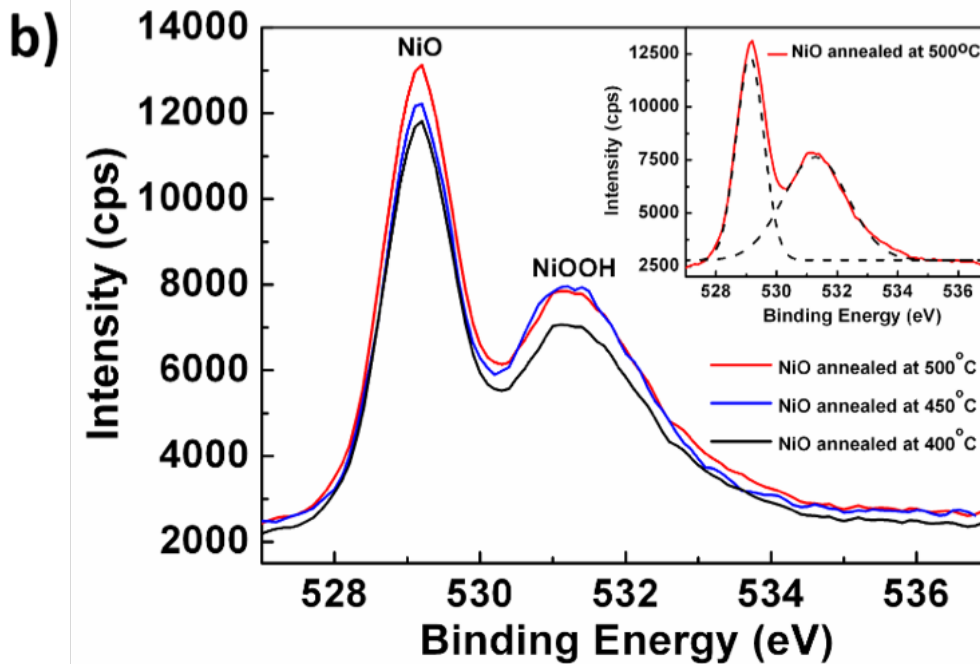


**Figure 3.7.** Regional XPS spectra for (a) Ni 2p and (b) O 1s core levels of the NiO thin films annealed in air at different temperatures.

### 3.2. Optical Properties of NiO Thin Films: UV-Vis Analyses

Optical transmission spectra of the films are provided separately in Figures 3.8. (a)-(c). Optical transmittance of 60 nm thick films is approximately 80%; while that of 110 and 170 nm films are 75% and 65%, respectively at the visible region of the spectrum.

There is a thickness dependent decrease in the transmission; however, annealing temperature has no effect on the optical transmission spectra of the films. From spectral transmission of NiO thin films, absorption coefficient ( $\alpha$ ) has been estimated using the Lambert formula:

$$\alpha = \frac{1}{t} \ln \left( \frac{1}{T} \right)$$

, where,  $t$  is the film thickness and  $T$  is the transmittance. Absorption behavior of NiO films exhibits Urbach characteristic since the absorption coefficient decreases with a decrease in photon energy [121]. From absorption coefficient, optical band gap of the films was determined using Tauc's relation:

$$\alpha(\nu)h\nu = B(h\nu - E_{gap})^m$$

where,  $\alpha(\nu)$  is the absorption coefficient obtained from Lambert formula,  $h\nu$  is the incident photon energy,  $B$  is the characteristic constant independent of photon energy,  $E_{gap}$  is the optical band gap and  $m$  is an index which can have different values of 1/2, 3/2, 2 or 3 depending on the nature of the electronic transitions. By substituting the first equation as  $\alpha = (-\ln T)/t$  into the second one [122], the variation of  $(\alpha h\nu)^2$  versus  $h\nu$  for NiO films with thickness of 60, 100 and 170 nm is shown in Figure 3.9. (a)-(c), respectively.  $E_{gap}$  values of the films were determined by extrapolation of the linear portion of the plots. Optical band gaps for 60, 110 and 170 nm films were estimated as  $4.31 \pm 0.10$ ,  $3.89 \pm 0.10$  and  $3.75 \pm 0.10$  eV, respectively. Although band gap of NiO is known to range between 3.6 and 4.0 eV, optical absorption studies suggest that this range can extend up to 4.2 eV due to the non-stoichiometry [123]. Excess or deficiency in metal ions with respect to oxygen ions leading to a charge imbalance has a critical effect on the electrical conductivity due to the formation of new localized energy levels between the conduction band and the valence band [124].

The optical analyses show that the  $E_{gap}$  values are changing only marginally with annealing temperature [125], whereas the change in  $E_{gap}$  values are quite remarkable with an increase in film thickness. However, a strong dependence of  $E_{gap}$  on the film thickness is observed. In this work, it is evident that the optical band gap decreases with an increase in the number of coating layers. Film thickness dependent changes in  $E_{gap}$  can be explained by the quantum confinement effect. Apart from the quantum

confinement, presence of the amorphous state or structural defect (such as grain boundaries) are also considered as a reasons for the change in the optical band gap [126].

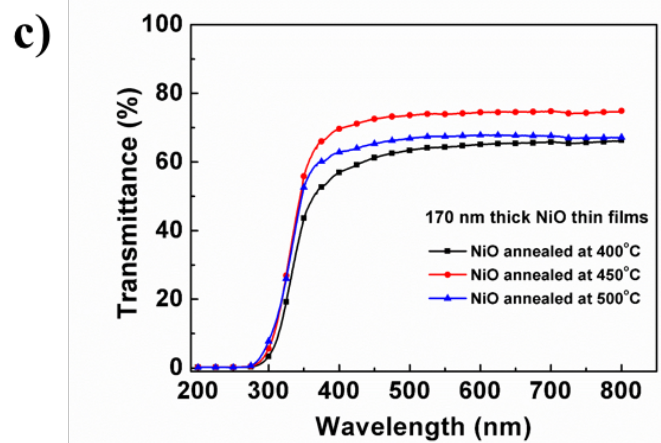
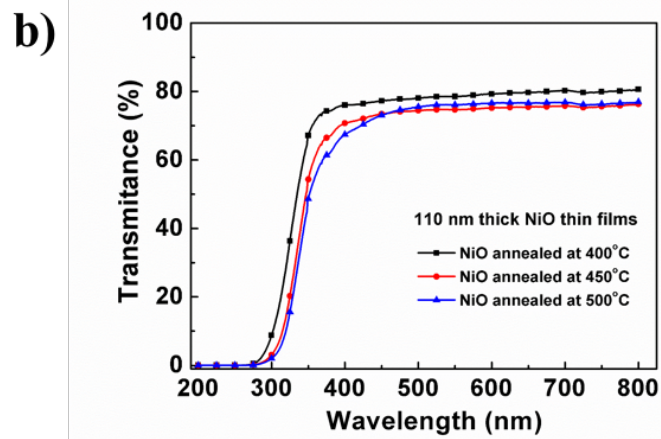
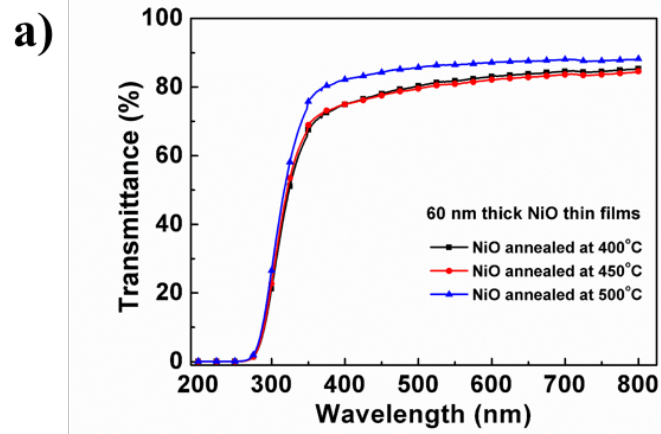


**Figure 3.8.** Optical transmission spectra of (a) 60, (b) 110 and (c) 170 nm thick NiO films annealed at 400, 450 and 500 °C.

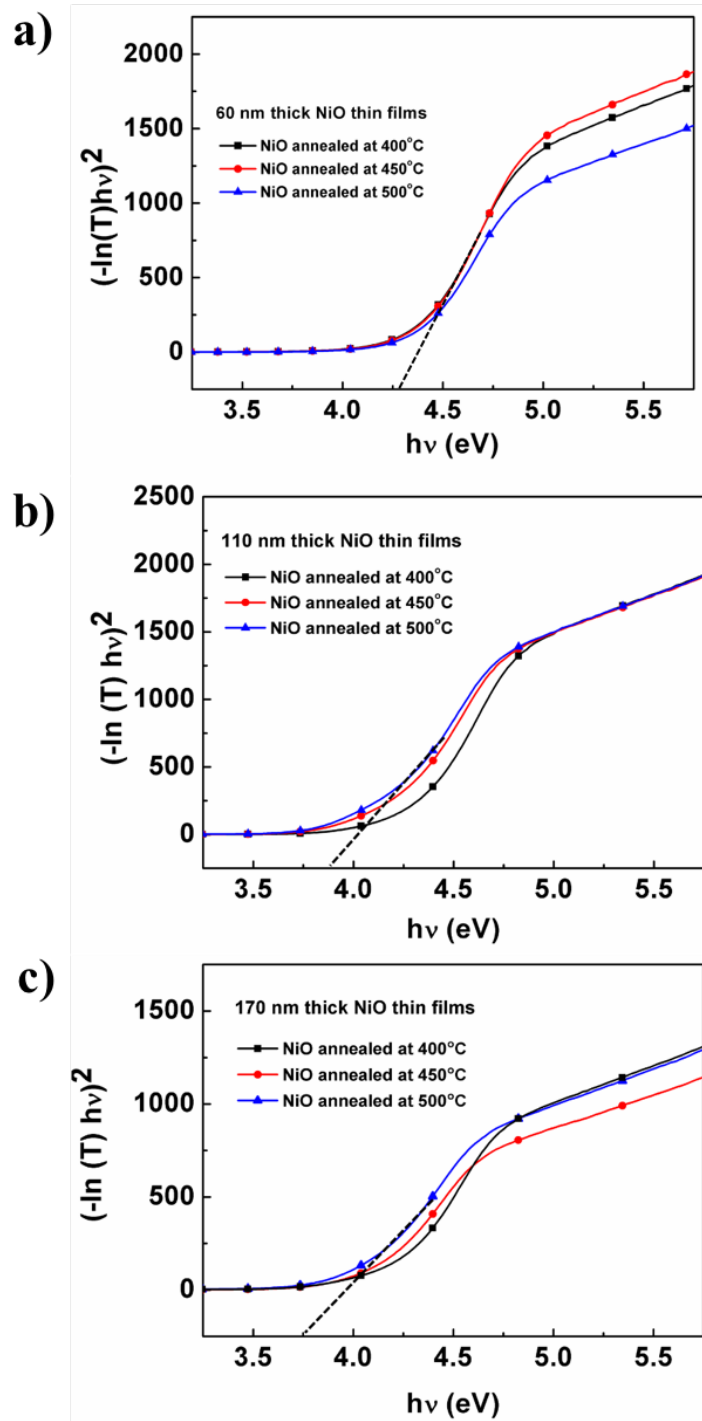


**Figure 3.9.** Optical band gap of (a) 60, (b) 110 and (c) 170 nm thick NiO films annealed at 400, 450 and 500 °C.

### **3.3. Electrical Properties of NiO Thin Films: Temperature-dependent Resistivity Measurements**

NiO is a first row transition metal monoxide and a p-type semiconductor. The predominant charge carriers creating the electrical conduction are holes. The electrical properties of pure stoichiometric NiO have been studied over the course of many years due to its attractive nature of the band structure [127]. Although it is theoretically expected that NiO conducts electricity as a transition metal oxide according to the conventional band theory, experimental studies reveal that it behaves as an excellent insulator [42]. The basic conceptual explanation of this contradiction between the experiments and the usual band theories was suggested by Mott [34]. In case of an extremely narrow band, Mott proposed electron-electron interactions and found out that the nature of NiO band structure prevents the conduction via 3d electrons due to the onsite Coulomb repulsion of extremely localized d-bands. Both theoretical and experimental studies concluded that the pure stoichiometric NiO obeys Mott-Hubbard model with a Mott-type correlation from 3d electrons [121]. NiO is an excellent insulator with a resistivity on the order of  $10^{13}$   $\Omega\text{cm}$  at room temperature and do not show thermally induced Mott transition [42]. In this study, to carry out the resistivity measurements, 170 nm thick films annealed at different temperatures were used. Room temperature resistivity of the films was found as  $1.7 \times 10^{12}$   $\Omega\text{cm}$  by a two probe technique which is 10 times lower compared to the pure stoichiometric structure. High conductivity is due to the surplus of  $\text{Ni}^{3+}$  as a result of monovalent impurities, nickel vacancies or oxygen interstitials on the lattice sites for p-type NiO [128]. Temperature-dependent resistivity of the 170 nm thick NiO films annealed at different temperatures is measured between 125 °C and 350 °C. Plots for the logarithmic scaled resistivities with respect to the reciprocal of the absolute temperature are given in Figure 3.10. (a)-(c).

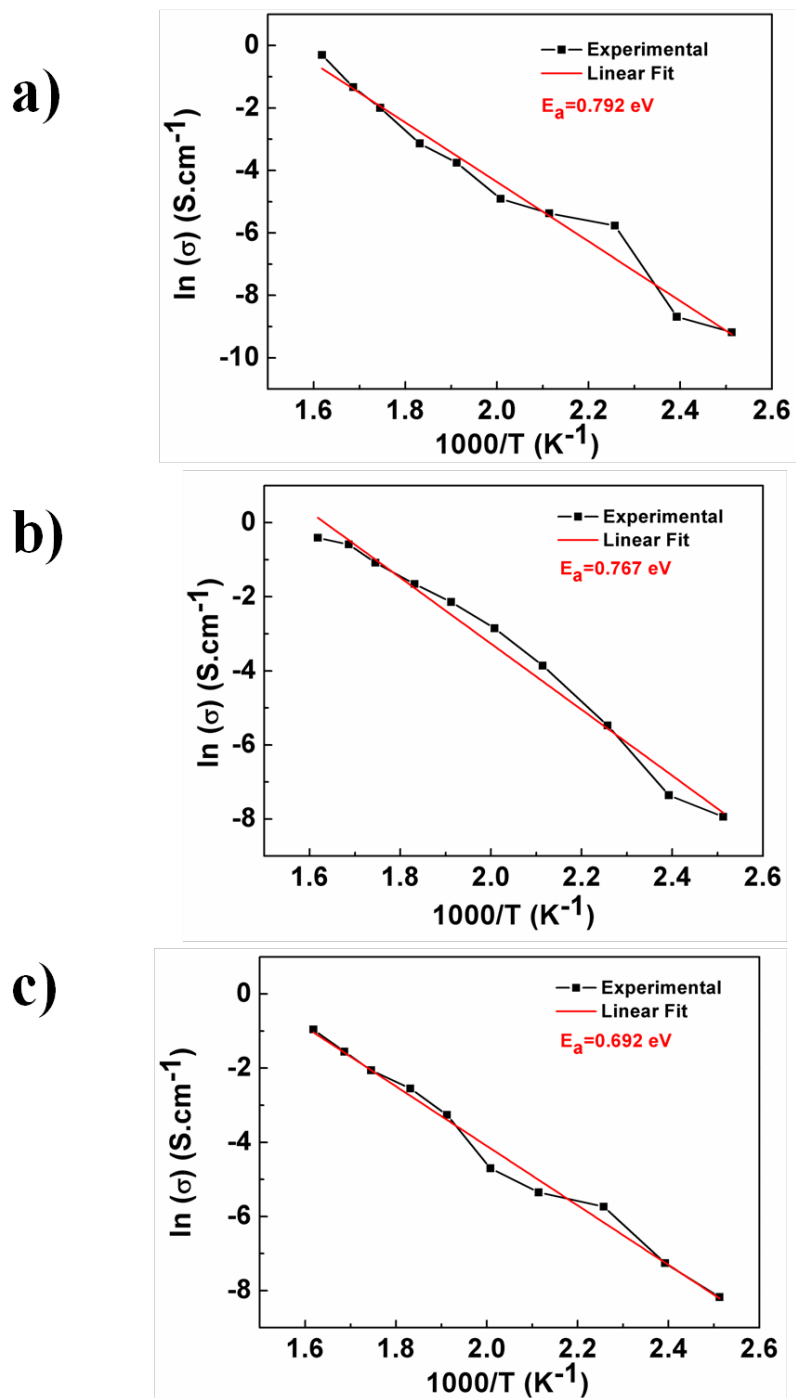


**Figure 3.10.** Temperature-dependent resistivity plots and the corresponding activation energies (in eV) for 170 nm thick NiO film annealed at (a) 400, (b) 450 and (c) 500 °C.

It was observed that the resistivity decreases from  $10^{12}$   $\Omega\text{cm}$  to  $10$   $\Omega\text{cm}$  with an increase in annealing temperature. Activation energies were calculated using the Arrhenius relation:

$$\sigma = Ae^{-E_a/2kT}$$

, where,  $\sigma$  is conductivity,  $A$  is a constant,  $T$  is the absolute temperature,  $k$  is the Boltzmann constant and  $E_a$  is the activation energy.  $E_a$  of NiO films annealed at 400, 450 and 500 °C were estimated to be 0.792, 0.767 and 0.692 eV, respectively. These results are in good agreement with the previous works; however, different activation energy values have also been reported before [109, 47, 129]. The difference in the activation energies can be due to the differences in the crystal structure, particle size and morphology. Slight decrease in the activation energy with annealing temperature observed herein can be explained by an increase in the particle size and decrease in the number of particle contacts. Thereby, charge carriers can move easily and find new pathways for the conduction, decreasing the activation energy. There are two competing conduction mechanisms for pure crystalline NiO below 1000 K. First one is due to small polarons in the 3d band of  $\text{O}^{2-}$  and the second one is due to large polarons in the 2p band of  $\text{O}^{2-}$  [130]. In the case of DC conductivity, activation energy of the thermally activated hopping, which gets originated by the small polarons were reported as 0.01 eV and it cannot be observed due to the low mobility of charge carriers [42]. Nevertheless, activation energy of the predominant band like (Arrhenius type) conduction due to large polarons between 200 and 1000 K is 0.6 eV, which is in agreement with activation energy observations reported in this study. So, temperature dependent resistivity changes and resultant activation energies indicate that the conductivity of NiO changes through Arrhenius type conduction mechanism. The activation energies for different temperature ranges were previously reported [40, 131]. For bulk NiO between 200 and 500 K activation energy is approximately 0.9 eV. 523 K is the Néel temperature ( $T_N$ ) corresponding to the antiferromagnetic to paramagnetic transition and above 523 K, activation energy decreases to 0.6 eV [42].

However, no change in the activation energy at Néel temperature was observed in this study. It was reported that the Néel temperature of nanosized NiO could be much lower than that of the bulk (i.e. 56 K [132]). This reveals that the magnetic properties of nanosized NiO is different from than its bulk counterparts. Therefore it is possible to have minor differences in activation energies of nanosized NiO and its bulk counterparts.

## CHAPTER 4

### CONCLUSIONS

NiO thin films with thicknesses in the range of 60 to 170 nm were formed on glass substrates by spin coating of sol-gel derived solutions. The films were crystalline NiO and no other secondary phases were observed. The crystal quality was found to improve with thermal treatment in the range of 400-500 °C.

Microstructural/morphological analytical findings revealed that the average particle size of nanostructured films increases in the range of 10-30 nm depending on annealing temperature.

Films were transparent in the visible region and their transmittance decreased from 80 to 65% as the film thickness increases from 60 to 170 nm. It was found that the annealing temperature does not change the transparency of the films. Optical band gaps of the films were decreased from  $4.3 \pm 0.1$  to  $3.8 \pm 0.1$  eV with the increase in the film thickness from 60 to 170 nm. Resistivity of the films were measured as  $1.7 \times 10^{12}$   $\Omega\text{cm}$  at room temperature. Resistivity of the films were decreased to several  $\Omega\text{cms}$  when measured at 350 °C. From temperature-dependent resistivity measurements, activation energies of 170 nm thick films that are annealed at 400, 450 and 500 °C were found as 0.792 eV, 0.767 eV and 0.692 eV, respectively. The processing based findings provided here may guide studies on solution deposition of NiO thin films.



## REFERENCES

- [1] A. M. Soleimanpour and A. H. Jayatissa, "Preparation of nanocrystalline nickel oxide thin films by sol-gel process for hydrogen sensor applications," *Mater. Sci. Eng. C*, vol. 32, no. 8, pp. 2230–2234, 2012.
- [2] X. Wang, Y. Zhu, J. Yang, X. Lu and L. Wang, "Preparation of NiO Nanoparticles and Their Catalytic Activity in the Thermal Decomposition of Ammonium Perchlorate," *Thermochim. Acta.*, vol. 437, pp. 106–109, 2005.
- [3] J. Lin, S. Chen and F. Kai, "Electrochromic Properties of Nano-Composite Nickel Oxide Film," *Appl. Surf. Sci.*, vol. 254, pp. 3357–3363, 2008.
- [4] Y. M. Lu, W. S. Hwang, J. S. Yang and H. C. Chuang, "Properties of nickel oxide thin films deposited by RF reactive magnetron sputtering," *Thin Solid Films*, vol. 420–421, pp. 54–61, 2002.
- [5] M. D. Irwin, D. B. Buchholz, A. W. Hains, R. P. H. Chang and T. J. Marks, "Structural and electrical functionality of NiO interfacial films in bulk heterojunction organic solar cells," *Chem. Mater.*, vol. 23, no. 8, pp. 2218–2226, 2011.
- [6] M. Z. Sialvi, R. J. Mortimer, G. D. Wilcox, A. M. Teridi, T. S. Varley, K. G. U. Wijayantha and C. A. Kirk, "Electrochromic and colorimetric properties of nickel(II) oxide thin films prepared by aerosol-assisted chemical vapor deposition," *ACS Appl. Mater. Interfaces*, vol. 5, no. 12, pp. 5675–5682, 2013.
- [7] W. Guo, K. N. Hui, and K. S. Hui, "High conductivity nickel oxide thin films by a facile sol-gel method," *Mater. Lett.*, vol. 92, pp. 291–295, 2013.
- [8] R. Cerc Korošec, P. Bukovec, B. Pihlar, and J. Padežnik Gomilšek, "The role of thermal analysis in optimization of the electrochromic effect of nickel oxide thin films, prepared by the sol–gel method. Part I," *Thermochim. Acta*, vol. 402,

- pp. 57–67, 2003.
- [9] J. Y. Park, K. S. Ahn, Y. C. Nah, H. S. Shim, and Y. E. Sung, “Electrochemical and Electrochromic Properties of Ni Oxide Thin Films Prepared by a Sol–Gel Method,” *J. Sol-Gel Sci. Technol.*, vol. 31, no. 1–3, pp. 323–328, 2004.
- [10] A. A. Al-Ghamdi, W. E. Mahmoud, S. J. Yaghmour, and F. M. Al-Marzouki, “Structure and optical properties of nanocrystalline NiO thin film synthesized by sol-gel spin-coating method,” *J. Alloys Compd.*, vol. 486, no. 1–2, pp. 9–13, 2009.
- [11] J. L. Garcia-Miquel, Q. Zhang, S. J. Allen, A. Rougier, A. Blyr, H. O. Davies, A. C. Jones, T. J. Leedham, P. A. Williams and S. A. Imprey, “Nickel oxide sol-gel films from nickel diacetate for electrochromic applications,” *Thin Solid Films*, vol. 424, no. 2, pp. 165–170, 2003.
- [12] E. Ozkan Zayim, I. Turhan, F. Z. Tepehan, and N. Ozer, “Sol-gel deposited nickel oxide films for electrochromic applications,” *Sol. Energy Mater. Sol. Cells*, vol. 92, no. 2, pp. 164–169, 2008.
- [13] J. C. De Jesus, I. González, A. Quevedo, and T. Puerta, “Thermal decomposition of nickel acetate tetrahydrate: An integrated study by TGA, QMS and XPS techniques,” *J. Mol. Catal. A Chem.*, vol. 228, no. 1–2 SPEC. ISS., pp. 283–291, 2005.
- [14] J. R. Manders, S. Tsang, M. J. Hartel, T. Lai, S. Chen, C. M. Amb, J. R. Reynolds and F. So, “Solution-Processed Nickel Oxide Hole Transport Layers in High Efficiency Polymer Photovoltaic Cells,” *Structure*, pp. 2993–3001, 2013.
- [15] K. K. Purushothaman, S. Joseph Antony, and G. Muralidharan, “Optical, structural and electrochromic properties of nickel oxide films produced by sol-gel technique,” *Sol. Energy*, vol. 85, no. 5, pp. 978–984, 2011.
- [16] L. Derue, S. Olivier, D. Tondelier, T. Maindron, B. Geffroy and E. Ishow, “All-Solution-Processed Organic Light-Emitting Diodes Based on Photostable Photo-cross-linkable Fluorescent Small Molecules,” *ACS Appl. Mater.*

- Interfaces*, vol. 8, no. 25, pp. 16207–16217, 2016.
- [17] K. J. Patel, G. G. Bhatt, J. R. Ray, P. Suryavanshi, and C. J. Panchal, “All-inorganic solid-state electrochromic devices: a review,” *J. Solid State Electrochem.*, pp. 1–11, 2016.
- [18] K.-C. Wang, J.-Y. Jeng, P.-S. Shen, Y.-C. Chang, E. W.-G. Diao, C.-H.- Tsai, T.-Y. Chao, H.-C. Hsu, P.-Y. Lin, P. Chen, T.-F. Guo and T.-C. Wen, “p-type Mesoscopic nickel oxide/organometallic perovskite heterojunction solar cells,” *Sci. Rep.*, vol. 4, p. 4756, 2014.
- [19] K. Badeker, *Ann. Phys.*, vol. 22, p. 749, 1907.
- [20] G. Haacke, “Transparent conducting coatings,” *Ann. Rev. Mater. Sci.*, pp. 73–94, 1977.
- [21] F. U. Hamelmann, “Transparent Conductive Oxides in Thin Film Photovoltaics,” *J. Phys. Conf. Ser.*, vol. 559, p. 12016, 2014.
- [22] T. Minami, “Transparent conducting oxide semiconductors for transparent electrodes,” *Semicond. Sci. Technol.*, vol. 20, no. 4, pp. S35–S44, 2005.
- [23] C. G. Granqvist and A. Hultåker, “Transparent and conducting ITO films: new developments and applications,” *Thin Solid Films*, vol. 411, no. 1, pp. 1–5, 2002.
- [24] M. Takada, T. Kobayashi, T. Nagase, and H. Naito, “Inverted organic light-emitting diodes using different transparent conductive oxide films as a cathode Inverted organic light-emitting diodes using different transparent conductive oxide films as a cathode,” vol. 6, pp. 3–6, 2016.
- [25] M. Aleksandrova, “Oxide coatings on flexible substrates for electrochromic applications,” *J. Phys. Conf. Ser.*, vol. 559, no. 1, p. 12003, 2014.
- [26] X. Yu, T. J. Marks, and A. Facchetti, “Metal oxides for optoelectronic applications,” *Nat. Mater.*, vol. 15, no. 4, pp. 383–396, 2016.
- [27] K. H. L. Zhang, K. Xi, M. G. Blamire, and R. G. Egdell, “P-type transparent conducting oxides,” *J. Phys. Condens. Matter*, vol. 28, no. 38, p. 383002, 2016.
- [28] S. C. Dixon, D. O. Scanlon, C. J. Carmalt, and I. P. Parkin, “n-Type doped

- transparent conducting binary oxides: an overview,” *J. Mater. Chem. C*, vol. 419, no. 2, pp. 462–465, 2016.
- [29] P. P. Edwards, A. Porch, M. O. Jones, D. V. Morgan and R. M. Perks, “Basic materials physics of transparent conducting oxides,” *Dalt. Trans.*, pp. 2995–3002, 2004.
- [30] H. Peelaers, E. Kioupakis, and C. G. Van De Walle, “Fundamental limits on optical transparency of transparent conducting oxides: Free-carrier absorption in SnO<sub>2</sub>,” *Appl. Phys. Lett.*, vol. 100, no. 1, pp. 1–4, 2012.
- [31] T. Sato, H. Minami, T. Takata, S. and Yamada, “Transparent conducting p-type NiO thin films prepared by magnetron sputtering,” *Thin Solid Films*, vol. 236, pp. 27–31, 1993.
- [32] “Web Elements.” [Online]. Available: [https://www.webelements.com/compounds/nickel/nickel\\_oxide.html](https://www.webelements.com/compounds/nickel/nickel_oxide.html). [Accessed: 20-Dec-2016].
- [33] T. M. Schuler, D. L. Ederer, S. Itza-Ortiz, G. T. Woods, T. A. Callcott, and J. C. Woicik, “Character of the insulating state in NiO: A mixture of charge-transfer and Mott-Hubbard character,” *Phys. Rev. B - Condens. Matter Mater. Phys.*, vol. 71, no. 11, pp. 1–7, 2005.
- [34] N. F. Mott, “The Basis of the Electron Theory of Metals, with Special Reference to the Transition Metals,” *Proc. Phys. Soc. A*, vol. 62, pp. 416–422, 1949.
- [35] J. Hubbard, “Exchange splitting in ferromagnetic nickel,” *Proc. Phys. Soc.*, vol. 84, no. 4, pp. 455–464, 1964.
- [36] S. Lany, J. Osorio-Guillén, and A. Zunger, “Origins of the doping asymmetry in oxides: Hole doping in NiO versus electron doping in ZnO,” *Phys. Rev. B - Condens. Matter Mater. Phys.*, vol. 75, no. 24, pp. 1–4, 2007.
- [37] D. P. Snowden and H. Saltsburg, “Hopping conduction in NiO,” *Phys. Rev. Lett.*, vol. 14, no. 13, pp. 497–499, 1965.
- [38] H. J. Bosman, A. J., and van Daal, “Small-polaron versus band conduction in some transition-metal oxides,” *Adv. Phys.*, vol. 19, no. 77, pp. 1–117, 1970.

- [39] G. A. Sawatzky and J. W. Allen, "Magnitude and origin of the band gap in NiO," *Phys. Rev. Lett.*, vol. 53, no. 24, pp. 2339–2342, 1984.
- [40] H. J. Van Daal and A. J. Bosman, "Hall effect in CoO, NiO, and  $\alpha$ -Fe<sub>2</sub>O<sub>3</sub>," *Phys. Rev.*, vol. 158, no. 3, pp. 736–747, 1967.
- [41] F. J. Morin, "Electrical properties of NiO," *Phys. Rev.*, vol. 93, no. 6, pp. 1199–1204, 1954.
- [42] D. Adler and J. Feinleib, "Electrical and optical properties of narrow-band materials," *Phys. Rev. B*, vol. 2, no. 8, pp. 3112–3134, 1970.
- [43] R. W. Wright and J. P. Andrews, "Temperature Variation of the Electrical Properties of Nickel Oxide," *Proc. Phys. Soc. Sect. A*, vol. 62, no. 7, pp. 446–455, 1949.
- [44] S. C. Chen, C. K. Wen, T. Y. Kuo, W. C. Peng, and H. C. Lin, "Characterization and properties of NiO films produced by RF magnetron sputtering with oxygen ion source assistance," *Thin Solid Films*, vol. 572, pp. 51–55, 2014.
- [45] G. Parravano, "Thermoelectric Behavior of Nickel Oxide," *J. Chem. Phys.*, vol. 23, no. 1949, p. 5, 1955.
- [46] H. Schwab, G. M., Schmid, "Effect of Added Oxides on p Conducting Nickel Oxide," *J. Appl. Phys.*, pp. 426–428, 1962.
- [47] T. Dutta, P. Gupta, A. Gupta, and J. Narayan, "Effect of Li doping in NiO thin films on its transparent and conducting properties and its application in heteroepitaxial p-n junctions," *J. Appl. Phys.*, vol. 108, no. 8, 2010.
- [48] J. Van Elp, H. Eskes, P. Kuiper, and G. A. Sawatzky, "Electronic structure of Li-doped NiO," *Phys. Rev. B*, vol. 45, no. 4, pp. 1612–1622, 1992.
- [49] C. Bosman, A. J., Crevecoeur, "Mechanism of the Electrical Conduction in Li-Doped NiO," *Phys. Rev.*, vol. 144, no. 2, pp. 763–770, 1966.
- [50] V. Biju and M. Abdul Khadar, "DC conductivity of consolidated nanoparticles of NiO," *Mater. Res. Bull.*, vol. 36, no. 1–2, pp. 21–33, 2001.
- [51] R. Newman and R. Chrenko, "Optical properties of nickel oxide," *Phys. Rev.*, vol. 114, no. 6, pp. 1507–1513, 1959.

- [52] P. Lunkenheimer, A. Loidl, C. R. Ottermann, and K. Bange, "Correlated barrier hopping in NiO films," *Phys. Rev. B*, vol. 44, no. 11, pp. 5927–5930, 1991.
- [53] A. Fujimori and F. Minami, "Valence-band photoemission and optical absorption in nickel compounds," *Phys. Rev. B*, vol. 30, no. 2, pp. 957–971, 1984.
- [54] V. Scheidt, H. Globl, M. and Dose, "The oxidation of nickel: a study of empty electronic states by inverse photoemission and soft X-ray appearance potential microscopy," *Surf. Sci.*, vol. 112, pp. 97–110, 1981.
- [55] S. A. Tang and C. W. VanSlyke, "Organic Electroluminescent Diodes," *Appl. Phys. Lett.*, vol. 51, no. 12, p. 913, 1987.
- [56] S. Liu, R. Liu, Y. Chen, S. Ho, J. H. Kim, and F. So, "Nickel Oxide Hole Injection/Transport Layers for Efficient Solution- Processed Organic Light-Emitting Diodes," *Chem. Mater.*, vol. 26, pp. 4528–4534, 2014.
- [57] M. Cai, T. Xiao, E. Hellerich, Y. Chen, R. Shinar, and J. Shinar, "High-efficiency solution-processed small molecule electrophosphorescent organic light-emitting diodes," *Adv. Mater.*, vol. 23, no. 31, pp. 3590–3596, 2011.
- [58] G. Liaptsis and K. Meerholz, "Crosslinkable TAPC-based hole-transport materials for solution-processed organic light-emitting diodes with reduced efficiency roll-off," *Adv. Funct. Mater.*, vol. 23, no. 3, pp. 359–365, 2013.
- [59] I.-M. Chan and F. C. Hong, "Improved performance of the single-layer and double-layer organic light emitting diodes by nickel oxide coated indium tin oxide anode," *Thin Solid Films*, vol. 450, no. 2, pp. 304–311, 2004.
- [60] H. C. Im, D. C. Choo, T. W. Kim, J. H. Kim, J. H. Seo, and Y. K. Kim, "Highly efficient organic light-emitting diodes fabricated utilizing nickel-oxide buffer layers between the anodes and the hole transport layers," *Thin Solid Films*, vol. 515, no. 12, pp. 5099–5102, 2007.
- [61] J. M. Frost, K. T. Butler, F. Brivio, C. H. Hendon, M. Van Schilfgaarde, and A. Walsh, "Atomistic origins of high-performance in hybrid halide perovskite solar cells," *Nano Lett.*, vol. 14, no. 5, pp. 2584–2590, 2014.

- [62] H.-S. Kim, I. Mora-Sero, V. Gonzalez-Pedro, F. Fabregat-Santiago, E. J. Juarez-Perez, N.-G. Park and J. Bisquert, “Mechanism of carrier accumulation in perovskite thin-absorber solar cells,” *Nat. Commun.*, vol. 4, no. July 2015, p. 2242, 2013.
- [63] N. J. Jeon, J. H. Noh, W. S. Yang, Y. C. Kim, S. Ryu, J. Seo and S. I. Seok, “Compositional engineering of perovskite materials for high-performance solar cells,” *Nature*, vol. 517, no. 7535, pp. 476–480, 2015.
- [64] K. X. Steirer, P. F. Ndione, N. E. Widjonarko, M. T. Lloyd, J. Meyer, E. L. Ratcliff, A. Kahn, N. R. Armstrong, C. J. Curtis, D. S. Ginley, J. J. Berry and D. C. Olson, “Enhanced efficiency in plastic solar cells via energy matched solution processed NiO x interlayers,” *Adv. Energy Mater.*, vol. 1, no. 5, pp. 813–820, 2011.
- [65] M. D. Irwin, D. B. Buchholz, A. W. Hains, R. P. H. Chang, and T. J. Marks, “p-Type semiconducting nickel oxide as an efficiency-enhancing anode interfacial layer in polymer bulk-heterojunction solar cells,” *Proc. Natl. Acad. Sci.*, vol. 105, no. 8, pp. 2783–2787, 2008.
- [66] H. Kwon, H. Y. Lee, and J.-Y. Lee, “Structure and Characteristics of Li-Doped NiO Thin Films Prepared by Using Pulsed-Laser Deposition Process,” *J. Nanosci. Nanotechnol.*, vol. 14, no. 5, pp. 3473–3476, 2014.
- [67] S. O. Kasap and J. A. Rowlands, “X-ray photoconductors and stabilized a-Se for direct conversion digital flat-panel X-ray image-detectors,” *J. Mater. Sci. Mater. Electron.*, vol. 11, no. 3, pp. 179–198, 2000.
- [68] Y. Kuo and H. Nominanda, “Nonvolatile hydrogenated-amorphous-silicon thin-film-transistor memory devices,” *Appl. Phys. Lett.*, vol. 89, no. 17, pp. 1–4, 2006.
- [69] F. Liao, C. Chen, and V. Subramanian, “Organic TFTs as gas sensors for electronic nose applications,” *Sensors Actuators, B Chem.*, vol. 107, no. 2, pp. 849–855, 2005.
- [70] P. Estrela and P. Migliorato, “Chemical and biological sensors using

- polycrystalline silicon TFTs,” *J. Mater. Chem.*, vol. 17, no. 3, p. 219, 2007.
- [71] A. C. Tickle, *A New Approach to Microelectronics*. New York: Wiley, 1969.
- [72] X. Li, T. Lin, J. Shin, and J. Jang, “Solution processed p-channel oxide thin film transistor employing metal doped nickel oxide,” pp. 1221–1224, 2016.
- [73] S. Y. Kim, C. H. Ahn, J. H. Lee, Y. H. Kwon, S. Hwang, J. Y. Lee and H. K. Cho, “p-channel oxide thin film transistors using solution-processed copper oxide,” 2013.
- [74] A. Liu, G. Liu, H. Zhu, B. Shin, E. Fortunato, R. Martins and F. Shan, “Hole mobility modulation of solution-processed nickel oxide thin-film transistor based on high-k dielectric,” *Appl. Phys. Lett.*, vol. 108, no. 23, 2016.
- [75] D. Monk, P. Mortimer and R. Rosseinsky, *Electrochromism and Electrochromic Devices*. Cambridge University Press, 2007.
- [76] S. Årman, “Electrochromic materials for display applications: An introduction,” *J. New Mater. Electrochem. Syst.*, vol. 4, no. 3, pp. 173–179, 2001.
- [77] D. F. Goodchild, R. G., Webb, J. B., Williams, “Electrical Properties of Highly Conducting and Transparent Thin Films of Magnetron Sputtered SnO<sub>2</sub>,” *J. Appl. Phys.*, vol. 57, no. 2308, 1985.
- [78] H. Huang, J. Tian, W. K. Zhang, Y. P. Gan, X. Y. Tao, X. H. Xia and J. P. Tu, “Electrochromic properties of porous NiO thin film as a counter electrode for NiO/WO<sub>3</sub> complementary electrochromic window,” *Electrochim. Acta*, vol. 56, no. 11, pp. 4281–4286, 2011.
- [79] M. Fantini, M. C. A., Gorenstein, A., Shen, W. M., Tomkiewicz, “Electroreflectance and photoresponse of NiO<sub>x</sub> thin films,” *SPIE Proc.*, vol. 1728, no. 41, 1992.
- [80] S. Pilban Jahromi, N. M. Huang, A. Kamalianfar, H. N. Lim, M. R. Muhamad, and R. Yousefi, “Facile synthesis of porous-structured nickel oxide thin film by pulsed laser deposition,” *J. Nanomater.*, vol. 2012, 2012.
- [81] D. Franta, B. Negulescu, L. Thomas, P. R. Dahoo, M. Guyot, I. Ohlídal, J. Mistrík and T. Yamaguchi “Optical properties of NiO thin films prepared by

- pulsed laser deposition technique,” *Appl. Surf. Sci.*, vol. 244, no. 1–4, pp. 426–430, 2005.
- [82] Y. Kakehi, S. Nakao, K. Satoh, and T. Kusaka, “Room-temperature epitaxial growth of NiO(111) thin films by pulsed laser deposition,” *J. Cryst. Growth*, vol. 237–239, pp. 591–595, 2002.
- [83] P. R. Willmott and J. R. Huber, “Pulsed laser vaporization and deposition,” *Rev. Mod. Phys.*, vol. 72, no. 1, pp. 315–328, 2000.
- [84] “Schwarz Group.” [Online]. Available: [http://groups.ist.utl.pt/rschwarz/rschwarzgroup\\_files/PLD\\_files/PLD.htm](http://groups.ist.utl.pt/rschwarz/rschwarzgroup_files/PLD_files/PLD.htm). [Accessed: 22-Dec-2016].
- [85] D. Depla, S. Mahieu, and J. Greene, “Sputter deposition processes,” *Handb. Depos. Technol. Film. coatings*, vol. 281, pp. 253–296, 1991.
- [86] I. Hotovy, J. Liday, H. Sitter, and P. Vogrinčič, “Properties of sputtered NiO thin films,” *J. Electr. Eng.*, vol. 53, no. 11, pp. 11–12, 2002.
- [87] J. Peng, Z. Xu, S. Wang, Q. Jie, and C. Chen, “Preparation and performance of nickel oxide films by ion beam sputtering deposition and oxidation annealing,” vol. 22, no. 8, pp. 409–416, 2010.
- [88] R. Lo Nigro, S. Battiato, G. Greco, P. Fiorenza, F. Roccaforte, and G. Malandrino, “Metal organic chemical vapor deposition of nickel oxide thin films for wide band gap device technology,” *Thin Solid Films*, vol. 563, pp. 50–55, 2014.
- [89] D. Perednis and L. J. Gauckler, “Thin film deposition using spray pyrolysis,” *J. Electroceramics*, vol. 14, no. 2, pp. 103–111, 2005.
- [90] “TU Wien.” [Online]. Available: <http://www.iue.tuwien.ac.at/phd/filipovic/node56.html>. [Accessed: 21-Dec-2016].
- [91] A. E. Danks, S. R. Hall, and Z. Schnepp, “The evolution of ‘sol–gel’ chemistry as a technique for materials synthesis,” *Mater. Horiz.*, vol. 3, no. 2, pp. 91–112, 2016.

- [92] C. Brinker and G. Scherer, "Sol-Gel Science: The Physics and Chemistry of Sol-Gel Processing," *Advanced Materials*, vol. 3, no. 10. Academic Press, New York, p. 912, 1990.
- [93] A. C. Pierre, *Introduction to Sol-gel Processing*, 1st edition. Springer Science+Business Media New York Originally, 1998.
- [94] "Centexbel, Textile Competence Centre." AvailableL <http://www.centexbel.be> [Accessed: 22-Dec-2016]
- [95] "Nadotech Innovations." [Online]. Available: <http://www.nadotech.com/index.php/en/technologies>. [Accessed: 21-Dec-2016].
- [96] "Spin coater." [Online]. Available: <http://www.spincoater.com/what-is-spin-coating.php>. [Accessed: 22-Dec-2016].
- [97] P. A. Williams, A. C. Jones, J. F. Bickley, A. Steiner, H. O. Davies, T. J. Leedham, S. A. Impey, J. Garcia, S. Allen, A. Rougier and A. Blyr, "Synthesis and crystal structures of dimethylaminoethanol adducts of Ni(II) acetate and Ni(II) acetylacetonate. Precursors for the sol-gel deposition of electrochromic nickel oxide thin films," *J. Mater. Chem.*, vol. 11, no. 9, pp. 2329–2334, 2001.
- [98] S. H. Park, J. W. Lim, S. J. Yoo, I. Y. Cha, and Y. E. Sung, "The improving electrochromic performance of nickel oxide film using aqueous N,N-dimethylaminoethanol solution," *Sol. Energy Mater. Sol. Cells*, vol. 99, pp. 31–37, 2012.
- [99] C. Cantalini, M. Post, D. Buso, M. Guglielmi, and a. Martucci, "Gas sensing properties of nanocrystalline NiO and Co<sub>3</sub>O<sub>4</sub> in porous silica sol-gel films," *Sensors Actuators B Chem.*, vol. 108, no. 1–2, pp. 184–192, 2005.
- [100] P. K. Sharma, M. C. A. Fantini and A. Gorenstein, "Synthesis , characterization and electrochromic properties of NiO<sub>x</sub>H<sub>y</sub> thin film prepared by a sol-gel method," *Solid State Ionics*, vol. 115, pp. 457–463, 1998.
- [101] B. T. Raut, S. G. Pawar, M. A. Chougule, S. Sen, and V. B. Patil, "New process for synthesis of nickel oxide thin films and their characterization," *J. Alloys*

- Compd.*, vol. 509, no. 37, pp. 9065–9070, 2011.
- [102] S. R. Nalage, M. A. Chougule, S. Sen, P. B. Joshi, and V. B. Patil, “Sol-gel synthesis of nickel oxide thin films and their characterization,” *Thin Solid Films*, vol. 520, no. 15, pp. 4835–4840, 2012.
- [103] E. Scolan and C. Sanchez, “Synthesis and Characterization of Surface-Protected Nanocrystalline Titania Particles,” *Chem. Mater.*, vol. 10, no. 14, pp. 3217–3223, 1998.
- [104] A. Surca, B. Orel, B. Pihlar, and P. Bukovec, “Optical, spectroelectrochemical and structural properties of sol-gel derived Ni-oxide electrochromic film,” *J. Electroanal. Chem.*, vol. 408, no. 1–2, pp. 83–100, 1996.
- [105] A. Šurca, B. Orel, and B. Pihlar, “Sol-gel derived hydrated nickel oxide electrochromic films: Optical, spectroelectrochemical and structural properties,” *J. Sol-Gel Sci. Technol.*, vol. 8, no. 1–3, pp. 743–749, 1997.
- [106] S. Dendouga, S., Benramache and S., Lakel, “Influence of Film Thickness on Optical and Electrical Properties of Nickel Oxide (NiO) Thin Films,” *J. Chem. Mater. Res.*, vol. 5, no. 4, pp. 78–84, 2016.
- [107] M. Kondoh, K. and Mizuhashi, “Surface treatment of sheet glass. Present status and future prospects,” *J. Non. Cryst. Solids*, vol. 178, pp. 189–198, 1994.
- [108] M. Jlassi, I. Sta, M. Hajji, and H. Ezzaouia, “Optical and electrical properties of nickel oxide thin films synthesized by sol-gel spin coating,” *Mater. Sci. Semicond. Process.*, vol. 21, no. 1, pp. 7–13, 2014.
- [109] S. A. Mahmoud, A. A. Akl, H. Kamal, and K. Abdel-Hady, “Opto-structural, electrical and electrochromic properties of crystalline nickel oxide thin films prepared by spray pyrolysis,” *Phys. B Condens. Matter*, vol. 311, no. 3–4, pp. 366–375, 2002.
- [110] I. Sta, M. Jlassi, M. Hajji, and H. Ezzaouia, “Structural, optical and electrical properties of undoped and Li-doped NiO thin films prepared by sol-gel spin coating method,” *Thin Solid Films*, vol. 555, pp. 131–137, 2014.
- [111] Z. M. Jarzebski, *Oxide Semiconductors*. Oxford: Pergamon Press, 1974.

- [112] M. Ahmadi, R. Younesi, T. Vegge, and M. J.-F. Guinel, “Nickel oxide crystalline nano flakes: synthesis, characterization and their use as anode in lithium-ion batteries,” *Mater. Res. Express*, vol. 1, no. 2, p. 25501, 2014.
- [113] L. G.. Teoh, and K.-D. Li, “Synthesis and characterization of NiO nanoparticles by sol – gel method,” vol. 53, no. 3, pp. 2135–2140, 2012.
- [114] N. Mironova-Ulmane, A. Kuzmin, I. Steins, J. Grabis, I. Sildos, and M. Pärns, “Raman scattering in nanosized nickel oxide NiO,” *J. Phys. Conf. Ser.*, vol. 93, no. December, p. 12039, 2007.
- [115] M. T. Hutchings and E. J. Samuelsen, “Measurement of spin-wave dispersion in NiO by inelastic neutron scattering and its relation to magnetic properties,” *Phys. Rev. B*, vol. 6, no. 9, pp. 3447–3461, 1972.
- [116] N. Mironova-Ulmane, A. Kuzmin, J. Grabis, I. Sildos, V. I. Voronin, I. F. Berger and V. A. Kazantsev, “Structural and magnetic properties of nickel oxide nanopowders,” *Solid State Phenom.*, vol. 168–169, pp. 341–344, 2011.
- [117] E. Cazanelli, A. Kuzmin, G. Mariotto and N. Mironova-Ulmane, “Study of vibrational and magnetic excitations in Ni<sub>c</sub>Mg<sub>1-c</sub>O solid solutions by Raman spectroscopy,” *J. Phys. Condens. Matter*, vol. 15, no. 12, p. 2045, 2003.
- [118] W. J. Duan, S. H. Lu, Z. L. Wu, and Y. S. Wang, “Size effects on properties of NiO nanoparticles grown in alkalisalts,” *J. Phys. Chem. C*, vol. 116, no. 49, pp. 26043–26051, 2012.
- [119] V. Gowthami, P. Perumal, R. Sivakumar, and C. Sanjeeviraja, “Structural and optical studies on nickel oxide thin film prepared by nebulizer spray technique,” *Phys. B Condens. Matter*, vol. 452, pp. 1–6, 2014.
- [120] M. C. Biesinger, B. P. Payne, L. W. M. Lau, A. Gerson, and R. S. C. Smart, “X-ray photoelectron spectroscopic chemical state quantification of mixed nickel metal, oxide and hydroxide systems,” *Surf. Interface Anal.*, vol. 41, no. 4, pp. 324–332, 2009.
- [121] D. P. Joseph, M. Saravanan, B. Muthuraaman, P. Renugamball, S. Sambasivam, S. P. Raja, P. Maruthamuthu and C. Venkateswaran, “Spray deposition and

- characterization of nanostructured Li doped NiO thin films for application in dye-sensitized solar cells.,” *Nanotechnology*, vol. 19, no. 48, p. 485707, 2008.
- [122] A. Mahmood, U. Aziz, R. Rashid, A. Shah, Z. Ali, Q. Raza, M. Raffi and I. Shakir “Exploration of optical behavior of  $Cd_{1-x}Ni_xTe$  thin films by spectroscopic ellipsometry,” *Mater. Res. Express*, vol. 1, no. 4, p. 46409, 2014.
- [123] J. Feinleib and D. Adler, “Band structure and electrical conductivity of NiO,” *Phys. Rev. Lett.*, vol. 21, no. 14, pp. 1010–1013, 1968.
- [124] J. A. Dirksen, K. Duval, and T. A. Ring, “NiO thin-film formaldehyde gas sensor,” *Sensors Actuators, B Chem.*, vol. 80, no. 2, pp. 106–115, 2001.
- [125] H. L. Lu, G. Scarel, M. Alia, M. Fanciulli, S. J. Ding, and D. W. Zhang, “Spectroscopic ellipsometry study of thin NiO films grown on Si (100) by atomic layer deposition,” *Appl. Phys. Lett.*, vol. 92, no. 22, pp. 2006–2009, 2008.
- [126] E. S. M. Goh, T. P. Chen, C. Q. Sun, and Y. C. Liu, “Thickness effect on the band gap and optical properties of germanium thin films,” *J. Appl. Phys.*, vol. 107, no. 2, pp. 1–5, 2010.
- [127] S. O. F. Manghi, C. Calandra, “Quasiparticle Band Structure of NiO: Mott-Hubbard picture regained,” *Phys. Rev. Lett.*, vol. 73, no. 18, pp. 3129–32, 1994.
- [128] M. R. da Silva, L. V. A. Scalvi, L. H. Dall’Antonia, and D. I. dos Santos, “Deposition and photo-induced electrical resistivity of dip-coated NiO thin films from a precipitation process,” *J. Mater. Sci. Mater. Electron.*, vol. 24, no. 6, pp. 1823–1831, 2013.
- [129] P. S. Patil and L. D. Kadam, “Preparation and characterization of spray pyrolyzed nickel oxide (NiO) thin films,” *Appl. Surf. Sci.*, vol. 199, no. 1–4, pp. 211–221, 2002.
- [130] V. Biju and M. Abdul Khadar, “AC conductivity of nanostructured nickel oxide,” *J. Mater. Sci.*, vol. 36, no. 24, pp. 5779–5787, 2001.
- [131] M. Bransky, I. Tallan, “High-temperature defect structure and electrical properties of NiO,” *J. Chem. Phys.*, vol. 49, p. 1243, 1968.

- [132] M. Tadic, D. Nikolic, M. Panjan, and G. R. Blake, “Magnetic properties of NiO (nickel oxide) nanoparticles : Blocking temperature and Neel temperature,” *J. Alloys Compd.*, vol. 647, pp. 1061–1068, 2015.